

國立臺灣大學工學院土木工程學系



碩士論文

Department of Civil Engineering

College of Engineering

National Taiwan University

Master Thesis

以局部徑向基底函數佈點法分析

三維功能梯度壓電半導體問題

Three-dimensional Analysis for Functionally Graded  
Piezoelectric Semiconductors by the Local Radial Basis  
Function Collocation Method

陸學賢

Hubert Hsueh-Hsien Lu

指導教授：楊德良 博士

Advisor: Der-Liang Young, Ph.D.

中華民國 105 年 7 月

July, 2016

# 審定書



國立臺灣大學（碩）博士學位論文  
口試委員會審定書  
以局部徑向基底函數佈點法分析  
三維功能梯度壓電半導體問題  
Three-dimensional Analysis for Functionally Graded  
Piezoelectric Semiconductors by the Local Radial Basis  
Function Collocation Method

本論文係陸學賢君（R03521324）在國立臺灣大學土木工程學系碩士班完成之碩士學位論文，於民國 105 年 01 月 25 日承下列考試委員審查通過及口試及格，特此證明

口試委員：

楊 德 良

(指導教授)

洪 宏 基

陳 東 陽

陳 正 宗

郭 心 怡

系主任

呂 良 正

(簽名)

## 致謝



首先感謝指導教授楊德良老師非常有耐心的指導我，從一個什麼都不懂的大學畢業生，到現在對自己研究生生涯感到驕傲，老師不僅在學術方面給予指導，甚至在做人處事上都相當關心學生我，也改正了我不少壞習慣。起初，參與壓電材料的數值模擬計畫時相當的不開心，那時覺得我自己身為一個水利組的學生就應該做和流體力學或水利工程相關的研究，但在老師的循循善誘下，我漸漸地珍惜這個能跨領域學習的機會，在碩一升碩二的暑假甚至還讓研究生的我能到斯洛伐克參加學術交流，非常感謝老師讓我加入這個研究團隊，往後學生也將更努力地學習。

接著我想感謝 Sladek 教授的建議和指導，還有其團隊成員 Peter，非常有耐心積極的指正我對學理上的錯誤，一來一往百餘篇的電子郵件讓我非常感激。另外特別感謝口試委員們提供給我許多寶貴的意見，讓我能在研究和論文上更精進更完整。此外非常感謝學長吳清森博士不管在學術或是在遇到問題時該如何面對上都給我許多意見和幫助，也感謝研究室學長姐們在我剛進團隊時非常有耐心的教我，從一個程式都不會到 MATLAB、C++ 都相當熟悉。感謝研究室的學弟們、助理，Mahmoud 讓我練習英文口說還有亂扯紓解壓力，也感謝我同屆的研究室好麻吉們，祝大家順利畢業。最後感謝我的家人們，總是支持我一切決定，就像隱形的翅膀一樣讓我走到今天，在我徬徨失落的時候給我依靠，希望以後我也能成為你們信任安心的依靠，並且實現自己的夢想。

## 摘要



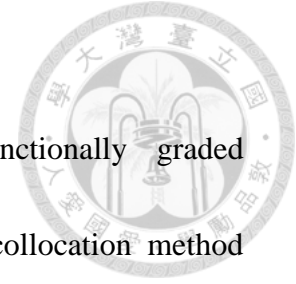
本研究主旨為藉由局部徑向基底函數佈點法分析三維梯度功能壓電半導體問題。局部徑向基底函數無網格數值方法已經被廣泛運用在工程與科學領域上，由於在處理空間尺度相差甚異與無須數值積分的優勢下，因此將此數值方法運用在壓電材料的工程問題上。

壓電材料可以分為介電體與半導體兩類，不同於壓電絕緣體，由電子密度及電流所組成的電守恆式需被額外用以描述壓電半導體的現象，這也加深了彈性位移及電場間相互作用分析的複雜度。此研究以局部徑向基底函數佈點法來求解存在非定常數的偏微分方程，在物理場中的空間變化以多元二次曲面徑向基底函數近似；時變性的微分方程系統問題以 Houbolt 有限差分法求解。

以有限元素法之相對應結果來驗證局部徑向基底函數佈點法之結果，且分析在不同載重情形下分析的樑所產生的力學反應、電場、電流場間互相的關係。此外，此研究也分析梯度參數及初始電子密度所產生之影響。最後，暫態分析也在此研究的範疇中。

關鍵詞：局部徑向基底函數佈點法、功能梯度材料、壓電半導體、壓電效應、智能材料

## Abstract

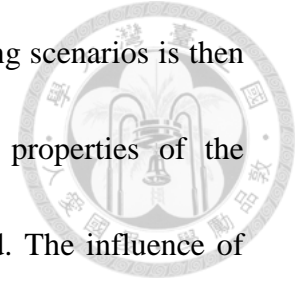


This thesis presents three-dimensional analysis of functionally graded piezoelectric semiconductor by the local radial basis function collocation method (LRBFCM). The LRBFCM is a commonly-used meshless numerical method in the field of engineering and sciences. On account of the advantages of addressing the problems with much different length scales in three dimensions and circumventing numerical quadrature, the LRBFCM is investigated and applied in the problems of piezoelectric materials.

Piezoelectric materials can be divided by dielectrics and semiconductors. Unlike piezoelectric dielectric materials, the conservation of charge which is composed of electron density and electric current is additionally considered to depict the phenomenon for piezoelectric semiconductors. This will complicate our analyzing the mutual coupling of elastic displacements and electric fields. For the solution of the set of partial differential equations with non-constant coefficients the LRBFCM is proposed in this work. The spatial variations of all physical fields are approximated by the multiquadric radial basis function. For time dependent problems a resulting system of ordinary differential equations is solved by the Houbolt finite difference scheme as a time stepping method.

The presented LRBFCM method is verified by using the corresponding results

obtained by the finite element method. The effect of various loading scenarios is then considered in the numerical examples to analyze the mutual properties of the mechanical responses, electrical fields, and electrical current field. The influence of material parameter gradation and initial electron density is then investigated. The transient analysis is also analyzed.



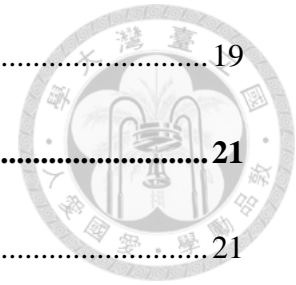
**Keywords:** local radial basis function collocation method (LRBFCM), functionally graded materials, piezoelectric semiconductors, piezoelectric effect, smart materials

# Table of Contents



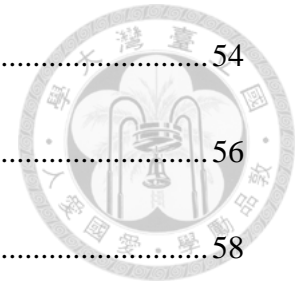
摘要.....	i
Abstract.....	ii
Table of Contents .....	iv
List of Figures .....	vii
List of Tables.....	xii
<b>Chapter 1      Introduction .....</b>	<b>1</b>
1.1      Motivations and Objectives .....	1
1.1.1 Mesh-dependent numerical methods .....	2
1.1.2 Meshless numerical methods .....	3
1.2      Organization of the thesis .....	4
<b>Chapter 2      The Local Radial Basis Function Collocation Method .....</b>	<b>7</b>
2.1      The radial basis function collocation method .....	8
2.2      The local radial basis function collocation method .....	9
2.3      Radial basis function .....	12
2.4      Local influence area .....	15
2.5      Shape parameter .....	18
2.6      Normalization technique .....	19
2.6.1 Normalized distance .....	19

2.6.2 Normalized shape parameter .....	19
<b>Chapter 3 Piezoelectricity .....</b>	<b>21</b>
3.1 Historical overview .....	21
3.2 Principles of piezoelectric effect.....	22
3.3 Applications in civil engineering .....	24
3.4 Functionally graded materials.....	25
3.5 The constitutive equations of piezoelectric materials .....	26
<b>Chapter 4 The Local Radial Basis Function Collocation Method for</b>	
<b>Functionally Graded Piezoelectric Semiconductor.....</b>	<b>32</b>
4.1 Introduction.....	32
4.2 Governing equations .....	35
4.3 Boundary conditions and initial conditions .....	40
4.3.1 Boundary conditions.....	40
4.3.2 Initial conditions.....	44
4.4 Numerical solution by the local radial basis function collocation method .....	44
4.4.1 The transient analysis .....	44
4.4.2 The static analysis .....	48
4.5 Numerical examples.....	49
4.5.1 The validation of the LRBFCM .....	52

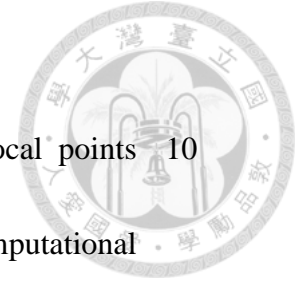




4.5.2 The influence of initial electron density .....	54
4.5.3 The influence of grading parameter .....	56
4.5.4 The influence of complex grading parameter .....	58
4.5.5 The transient analyses .....	61
<b>Chapter 5      Conclusions and Future Works .....</b>	<b>65</b>
5.1 Conclusions.....	65
5.2 Future Works.....	66
<b>Acknowledgement .....</b>	<b>67</b>
<b>References .....</b>	<b>68</b>
<b>Appendix.....</b>	<b>77</b>
A. Houbolt method.....	77
<b>Personal Information.....</b>	<b>78</b>



## List of Figures



- Fig.2.2.1 The illustration of a computation point with its local points 10  
respect to the local influence area  $\omega_i$  within the computational  
domain  $\Omega$ .
- Fig.2.4.1 The number of the nearest points with respect to every 16  
computation point by choosing  $NL = 5$  in the two-dimensional  
uniform point distribution case.
- Fig.2.4.2 The selection of points within the fixed radius in the two- 17  
dimensional non-uniform point distribution case.
- Fig.2.4.3 The cross-shaped selection 18
- Fig.3.2.1 The illustration of the relations between the energies and the 23  
piezoelectric effects.
- Fig.3.2.1 Configuration of the direct piezoelectric effect. (G: 24  
galvanometer)
- Fig.3.4.1 Configuration of two-layered composites and FGMs. 26
- Fig.4.5.1 The geometry of the beam. 50

Fig.4.5.2 The distribution of the points.

Fig.4.5.3 The illustration of the boundary conditions.



Fig.4.5.1.1 Variation of vertical displacement for a line along  $x_1$  and 53  
located at  $x_2 = 0$  and  $x_3 = h/2$  in the static analysis.

Fig.4.5.1.2 Variation of electric potential for a line along  $x_1$  and located at 53  
 $x_2 = 0$  and  $x_3 = h/2$  in the static analysis.

Fig.4.5.1.3 Variation of electron density for a line along  $x_1$  and located at 54  
 $x_2 = 0$  and  $x_3 = h/2$  in the static analysis.

Fig.4.5.2.1 Variation of vertical displacements along the line 55  
 $(x_1, x_2 = 0, x_3 = h/2)$  for different values of  $M_0$  in the beam  
under static load  $T_3 = 100\text{Pa}$  .

Fig.4.5.2.2 Variation of electric potential along the line 55  
 $(x_1, x_2 = 0, x_3 = h/2)$  for different values of  $M_0$  in the beam  
under static load  $T_3 = 100\text{Pa}$  .

Fig.4.5.2.3 Variation of electron density along the line 56  
 $(x_1, x_2 = 0, x_3 = h/2)$  for different values of  $M_0$  in the beam  
under static load  $T_3 = 100\text{Pa}$  .

Fig.4.5.3.1 Variation of vertical displacement along the line 57  
( $x_1, x_2 = 0, x_3 = h/2$ ) for different values of the gradation  
parameter  $\delta$  in the FGM beam under the static load  
 $T_3 = 100\text{Pa}$ .

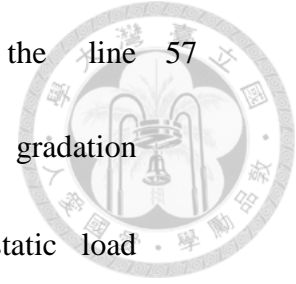


Fig.4.5.3.2 Variation of electric potential along the line 57  
( $x_1, x_2 = 0, x_3 = h/2$ ) for different values of the gradation  
parameter  $\delta$  in the FGM beam under the static load  
 $T_3 = 100\text{Pa}$ .

Fig.4.5.3.3 Variation of electron density along the line 58  
( $x_1, x_2 = 0, x_3 = h/2$ ) for different values of the gradation  
parameter  $\delta$  in the FGM beam under the static load  
 $T_3 = 100\text{Pa}$ .

Fig.4.5.4.1 Variation of vertical displacement along the line 59  
( $x_1, x_2 = 0, x_3 = h/2$ ) for the three combinations of the  
gradation of material coefficients in the FGM beam under static  
load  $T_3 = 100\text{Pa}$ .

Fig.4.5.4.2 Variation of electric potential along the line 60  
( $x_1, x_2 = 0, x_3 = h/2$ ) for the three combinations of the

gradation of material coefficients in the FGM beam under static

load  $T_3 = 100\text{Pa}$  .

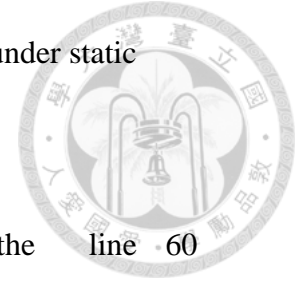


Fig.4.5.4.3 Variation of electron density along the line 60

$(x_1, x_2 = 0, x_3 = h/2)$  for the three combinations of the

gradation of material coefficients in the FGM beam under static

load  $T_3 = 100\text{Pa}$  .

Fig.4.5.5.1 Time evolution of vertical displacement along the line 62

$(x_1, x_2 = 0, x_3 = h/2)$  by the CT and BT methods for the first-

order temporal partial derivative under static and impact load

$T_3 = 100\text{Pa}$  .

Fig.4.5.5.2 Time evolution of electric potential along the line 62

$(x_1, x_2 = 0, x_3 = h/2)$  by the CT and BT methods for the first-

order temporal partial derivative under static and impact load

$T_3 = 100\text{Pa}$  .

Fig.4.5.5.3 Time evolution of vertical displacement along the line 63

$(x_1, x_2 = 0, x_3 = h/2)$  for the three combinations of the

gradation of material coefficients in the FGM beam under static

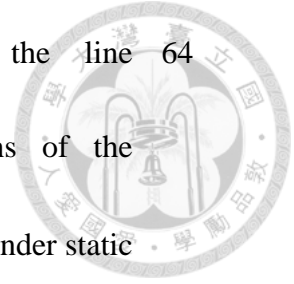
and impact load  $T_3 = 100\text{Pa}$  .

Fig.4.5.5.4 Time evolution of electric potential along the line 64

$(x_1, x_2 = 0, x_3 = h/2)$  for the three combinations of the

gradation of material coefficients in the FGM beam under static

and impact load  $T_3 = 100\text{Pa}$  .



## List of Tables

Table.2.3.1 List of commonly-used RBFs



13

Table.2.3.2 The differential formulation of the MQ-RBF

14

# Chapter 1 Introduction

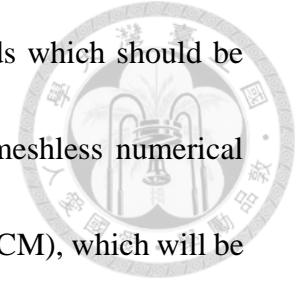


## 1.1 Motivations and Objectives

On account of the development of computer science and technology, numerical analyses have been frequently utilized and even substituted for some experiments. There are advantages by numerical analyses such as cheap and enable some problems which do not exist analytical solutions to be solved and analyzed. The numerical methods generally can be categorized as two types, mesh-dependent methods and meshless methods. Mesh-dependent methods have been developed and commonly used in scientific research and engineering applications. The following four mesh-dependent methods are most commonly used methods, the finite difference method (FDM), the finite volume method (FVM), the finite element method (FEM), and the boundary element method (BEM). However, the mesh-dependent numerical schemes still exist challenges and problems on account of inevitable burdensome tasks such as mesh generation and numerical quadrature especially for multi-dimensional problems and irregular domains. In order to avoid those problems, various meshless methods have been developed in recent years. They have become more and more popular due to the ease of implementation and the flexibility of generation of computational nodes which can circumvent the problems of inaccuracy near where gradients of variables are high.



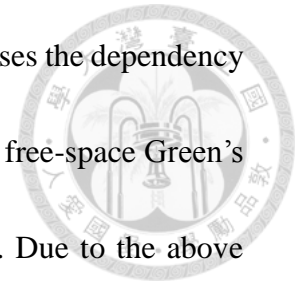
However, there are the stability and accuracy of meshless methods which should be concerned and analyzed. In this thesis, we focus on one of the meshless numerical methods, the local radial basis functions collocation method (LRBFCM), which will be introduced in subsection 1.1.2.



### **1.1.1 Mesh-dependent numerical methods**

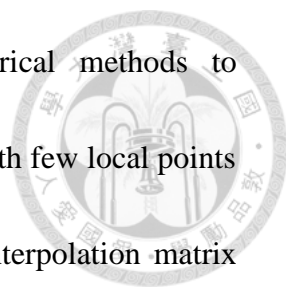
With the development of the computer technology in recent years, it has been more feasible and efficient to utilize numerical methods to simulate and analyze engineering problems. The finite difference method (FDM), the finite volume method (FVM), and the finite element method (FEM) have been developed to a robust and effective methods and widely used in engineering problems. The finite difference method is based on Taylor series expansion to approximate the derivative which accuracy is dependent on how many terms we utilize. However, it is complicated when we solve problems with irregular domain due to difficulty of construction of orthogonal mesh. Additionally, we should refine the mesh and add more terms of derivative to obtain more accurate results which is very time-consuming. In order to reduce the dependency of the meshes, researchers have developed a powerful alternative numerical scheme, the boundary element method (BEM), to substitute for other mesh-dependent numerical methods. By the Green's function, the BEM can reduce one dimensionality of the problems. The BEM discretizes the computational 3D domain of the surface instead of the whole

domain. Therefore, it provides more flexibility and relatively decreases the dependency of meshes. However, the limitation of the fundamental solutions or free-space Green's functions restricts engineers to apply the BEM to some problems. Due to the above difficulties of applying the mesh-dependent numerical methods, researchers have been paying attention on the development and improvement of meshless numerical methods.



### **1.1.2 Meshless numerical methods**

In order to circumvent numerical quadrature and mesh generation, various meshless or mesh-free numerical methods have been developed such as the smoothed particle hydrodynamics (SPH) [1], the multiquadrics collocation method (MQ) [2]-[6], the method of fundamental solutions (MFS) [7]-[10], the method of particular solutions (MPS) [11][12], the method of approximate particular solutions (MAPS) [13][14], the differential quadrature method (DQ) [15][16], the boundary particle method [17], and the finite point method (FPM) [18]. The above numerical methods are classified as global-type methods. Global-type methods generally utilize the discretization of all collocation points within the global domain. Subsequently, the problems such as the ill-conditioned and dense resultant interpolation matrix are inevitable. In order to improve the efficiency of computation and deal with large-scale problems, researchers have been developing various localization methods for the corresponding global-type numerical methods.



The localization technique allows the global-type numerical methods to approximate the solution of partial differential equations (PDEs) with few local points and then the individual relations constitute the sparse resultant interpolation matrix instead of the dense matrix. That enables computation procedures to utilize the solvers of inversion of sparse matrix and save substantial computational time and memory loading. The MQ, the MAPS, and the DQ are respectively improved and localized as the localized multiquadric method (LMQ) [19], the localized method of approximate particular solutions (LMAPS) [20]-[22], and the localized differential quadrature (LDQ) [23][24]. In addition, there are other localized meshless numerical methods such as the compactly supported radial basis functions [25], the local radial basis function collocation method (LRBFCM) [26]-[29], and the meshless local Petrov–Galerkin (MLPG) method [30][31]. This research will focus on the LRBFCM, and utilize it to conduct three-dimensional analysis for functionally graded piezoelectric semiconductors.

## **1.2 Organization of the thesis**

In order to analyze the functionally graded piezoelectric semiconductor problems by the local radial basis function method, we divide the thesis into five chapters and the brief introduction of them is shown as follows:

## ***Chapter 1 Introduction***



The motivation of this thesis is presented, and the difference between the mesh-dependent methods and meshless methods is also discussed in this chapter. In addition, the development of local meshless methods with respect to corresponding global-type meshless methods is mentioned.

## ***Chapter 2 The Local Radial Basis Function Collocation Method***

The meshless methods, the radial basis function collocation method (RBFCM) and the local radial basis function collocation method (LRBFCM), are introduced in this chapter.

## ***Chapter 3 Piezoelectricity***

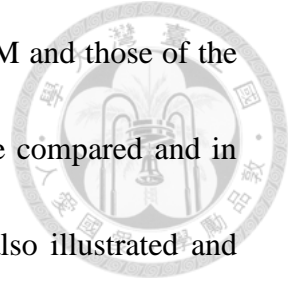
The piezoelectricity is introduced and can be divided by five sections, historical overview, principles of piezoelectric effect, applications in civil engineering, functionally graded materials, and the constitutive equations of piezoelectric materials.

## ***Chapter 4 The Local Radial Basis Function Collocation Method for***

### ***Functionally Graded Piezoelectric Semiconductor***

The LRBFCM is utilized to analyze the functionally graded piezoelectric

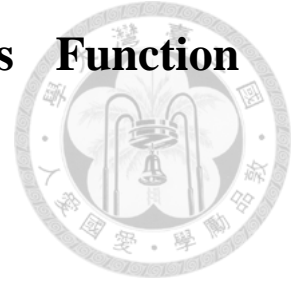
semiconductor problems in this chapter. The results of the LRBFCM and those of the finite element method by the commercial software, COMSOL, are compared and in good agreement. The effect of functionally graded properties is also illustrated and compared. The transient analyses are also analyzed in this chapter.



## ***Chapter 5 Conclusions and Future works***

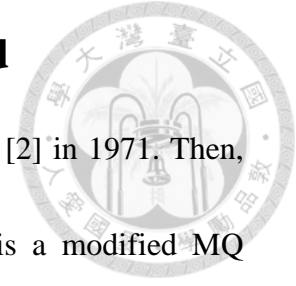
Conclusions and future works are summarized and proposed in this chapter, respectively.

# Chapter 2 The Local Radial Basis Function Collocation Method



This chapter will report the numerical tool, LRBFCM, which is utilized to deal with the piezoelectric sensor problem in this thesis. In the first section, we will illustrate the concept and the approximation procedure of the LRBFCM thoroughly. Then, we will introduce the RBFs which play an important role in the LRBFCM in the second section. Although the LRBFCM can overcome the drawbacks of the RBFCM, it is still a developing meshless numerical method whose stability and the accuracy should be further investigated. The accuracy and the stability in the LRBFCM is strongly depended on the selection of the supported local nodes and the value of the shape parameters. For the purpose of promoting the accuracy and the stability of the approximation results, we will introduce some kinds of methods for choosing the supported local nodes in the section 3 and the shape parameters in the section 4, respectively. In the last section, we provide the normalization technique to improve the multi-scale domain problems.

## 2.1 The radial basis function collocation method



The multiquadric (MQ) scheme was first proposed by Hardy [2] in 1971. Then, the radial basis function collocation method (RBFCM), which is a modified MQ scheme, was developed by Kansa. The RBFCM [3][4] requires a linear combination of radial basis functions with regard to all the computation points within the computational domain  $\Omega$  to approximate any given variable denoted by  $\phi$ . Let all the computation points be defined as  $\mathbf{x}_i \in \Omega, i \in [1, N]$ , where  $N$  is the total number of global points. Then the given variable at any computation point within the computational domain can be approximated by the following term

$$\phi(\mathbf{x}, t) = \sum_{k=1}^N \alpha_k f(\|\mathbf{x} - \mathbf{x}_k\|), \mathbf{x} \in \Omega \quad (2.1-1)$$

where  $f$  is the radial basis function,  $\alpha$  is the weighting coefficient to be determined, and  $\|\mathbf{x} - \mathbf{x}_k\|$  is the Euclidean distance between the global points. In order to evaluate the weighting coefficients, Eq. (2.1-1) at each computational point should be enforced.

Then, the system of the algebraic equations becomes

$$\boldsymbol{\phi} = \mathbf{f}\boldsymbol{\alpha}, \quad (2.1-2)$$

where  $\boldsymbol{\phi} = [\phi(\mathbf{x}_1, t), \dots, \phi(\mathbf{x}_N, t)]^T$ ,  $\boldsymbol{\alpha} = [\alpha_1, \dots, \alpha_N]^T$ , and

$$\mathbf{f} = \begin{bmatrix} f(\|\mathbf{x}_1 - \mathbf{x}_1\|) & f(\|\mathbf{x}_1 - \mathbf{x}_2\|) & \cdots & f(\|\mathbf{x}_1 - \mathbf{x}_N\|) \\ f(\|\mathbf{x}_2 - \mathbf{x}_1\|) & f(\|\mathbf{x}_2 - \mathbf{x}_2\|) & \cdots & f(\|\mathbf{x}_2 - \mathbf{x}_N\|) \\ \vdots & \vdots & \ddots & \vdots \\ f(\|\mathbf{x}_N - \mathbf{x}_1\|) & f(\|\mathbf{x}_N - \mathbf{x}_2\|) & \cdots & f(\|\mathbf{x}_N - \mathbf{x}_N\|) \end{bmatrix}.$$



To implement any given operator  $\zeta\{\}$ , the approximate summation equation of the variable in Eq. (2.1-1) becomes

$$\zeta\{\phi(\mathbf{x}, t)\} = \zeta\{\mathbf{f}\} \boldsymbol{\alpha}, \quad (2.1-3)$$

By solving Eq. (2.1-3), we obtain the weighting coefficient with respect to every computation point within the global domain. Then substituting the weighting coefficients into Eq. (2.1-1), we get the approximate values of the variable within the computational domain.

## 2.2 The local radial basis function collocation method

Due to time-consuming computation, large memory loading, dense and ill-conditioned resultant interpolation matrix, and sensitive shape parameter, the localization technique, the local radial basis function collocation method, was developed [26]. The local radial basis function collocation method (LRBFCM) enables engineers to analyze large-scale realistic problems and more efficiently compute partial differential equations by sparse solvers. Contrary to the RBFCM, LRBFCM utilizes the approximation of  $\phi(\mathbf{x}, t)$  with respect to the point  $\mathbf{x}_i, i \in [1, N]$  which is supported





by  $NL$  from the local influence area  $\omega_i$  as

$$\phi(\mathbf{x}, t) = \sum_{k=1}^{NL} \alpha_{i,k} f(\|\mathbf{x} - \mathbf{x}_{i,k}\|), \mathbf{x}_{i,k} \in \omega_i \quad (2.2-1)$$

where  $\alpha_{i,k}$  ( $i \in [1, N]; k \in [1, NL]$ ) are the weighting coefficients,  $f$  is the RBF, and  $\|\mathbf{x} - \mathbf{x}_{i,k}\|$  is the Euclidean distance between two points. In order to evaluate the weighting coefficients, Eq. (2.2-1) at each computational point from  $\omega_i$  should be enforced. Then, the system of the algebraic equations becomes

$$\boldsymbol{\phi}_i = \mathbf{f}_i \boldsymbol{\alpha}_i, \quad (2.2-2)$$

where  $\boldsymbol{\phi}_i = [\phi(\mathbf{x}_{i,1}, t), \dots, \phi(\mathbf{x}_{i,NL}, t)]^T$ ,  $\boldsymbol{\alpha}_i = [\alpha_{i,1}, \dots, \alpha_{i,NL}]^T$ , and

$$\mathbf{f}_i = \begin{bmatrix} f(\|\mathbf{x}_{i,1} - \mathbf{x}_{i,1}\|) & f(\|\mathbf{x}_{i,1} - \mathbf{x}_{i,2}\|) & \cdots & f(\|\mathbf{x}_{i,1} - \mathbf{x}_{i,NL}\|) \\ f(\|\mathbf{x}_{i,2} - \mathbf{x}_{i,1}\|) & f(\|\mathbf{x}_{i,2} - \mathbf{x}_{i,2}\|) & \cdots & f(\|\mathbf{x}_{i,2} - \mathbf{x}_{i,NL}\|) \\ \vdots & \vdots & \ddots & \vdots \\ f(\|\mathbf{x}_{i,NL} - \mathbf{x}_{i,1}\|) & f(\|\mathbf{x}_{i,NL} - \mathbf{x}_{i,2}\|) & \cdots & f(\|\mathbf{x}_{i,NL} - \mathbf{x}_{i,NL}\|) \end{bmatrix}.$$

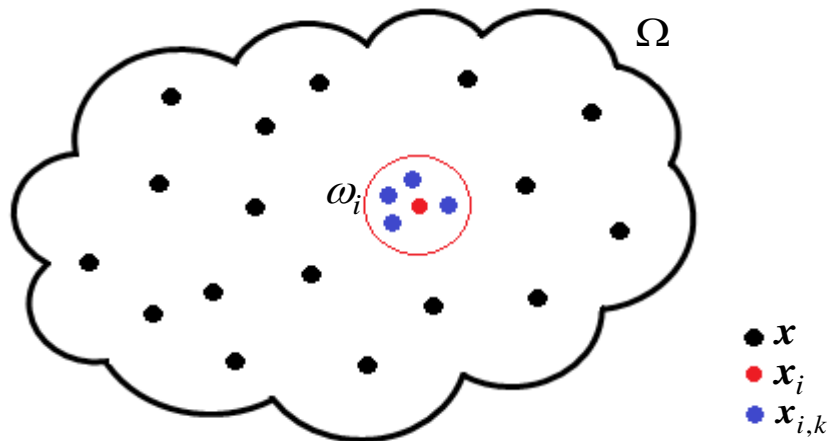


Fig.2.2.1 The illustration of a computation point with its local points respect to the local influence area  $\omega_i$  within the computational domain  $\Omega$ .

Since  $\mathbf{f}_i$  is invertible, the weighting coefficient can be determined as

$$\boldsymbol{\alpha}_i = \mathbf{f}_i^{-1} \boldsymbol{\phi}_i, i \in [1, N]. \quad (2.2-3)$$



Additionally, Eq. (2.2-1) can be rewritten as

$$\phi(\mathbf{x}, t) = \mathbf{F}_i(\mathbf{x}) \boldsymbol{\alpha}_i \quad (2.2-4)$$

by introducing the row-vector  $\mathbf{F}_i(\mathbf{x}) = [f(\|\mathbf{x} - \mathbf{x}_{i,1}\|), \dots, f(\|\mathbf{x} - \mathbf{x}_{i,NL}\|)]$ . To implement any given operator  $\zeta\{\cdot\}$ , the approximate summation equation of the variable in Eq. (2.2-1) gives

$$\zeta\{\phi(\mathbf{x}, t)\} = \sum_{k=1}^{NL} \alpha_{i,k} \zeta\{f(\|\mathbf{x} - \mathbf{x}_{i,k}\|)\} = \zeta\{\mathbf{F}_i(\mathbf{x})\} \boldsymbol{\alpha}_i \quad (2.2-5)$$

where  $\zeta\{\mathbf{F}_i(\mathbf{x}_i)\} = \zeta\{\mathbf{F}_i(\mathbf{x})\}|_{\mathbf{x}=\mathbf{x}_i}$ .

For convenience, we define the row vector  $(1 \times NL)$

$\mathbf{s}_i = \zeta\{\mathbf{F}_i(\mathbf{x}_i)\} \mathbf{f}_i^{-1} = [s_{i,1}, s_{i,2}, \dots, s_{i,NL}]$ , and then Eq. (2.2-5) becomes

$$\zeta\{\phi(\mathbf{x}_i, t)\} = \mathbf{s}_i \boldsymbol{\phi}_i, i \in [1, N]. \quad (2.2-6)$$

Subsequently, we transform the local system to the global system as shown in Eq. (2.2-6).

$$\zeta\{\phi(\mathbf{x}_i, t)\} = \mathbf{s}_i \boldsymbol{\phi}_i = \mathbf{S}_i \boldsymbol{\Phi}, i \in [1, N], \quad (2.2-7)$$

where

$$\mathbf{S}_i = [S_{i,1}, S_{i,2}, \dots, S_{i,N}], S_{i,j} = \begin{cases} 0, & \mathbf{x}_j \notin \omega_i \\ S_{i,j}, & \mathbf{x}_j \in \omega_i \end{cases}, \text{ and } \Phi = [\phi(\mathbf{x}_1, t), \phi(\mathbf{x}_2, t), \dots, \phi(\mathbf{x}_N, t)]^T.$$

Finally,

$$\zeta\{\Phi\} = \begin{bmatrix} \zeta\{\phi(\mathbf{x}_1, t)\} \\ \zeta\{\phi(\mathbf{x}_2, t)\} \\ \vdots \\ \zeta\{\phi(\mathbf{x}_N, t)\} \end{bmatrix} = \begin{bmatrix} \mathbf{S}_1 \Phi \\ \mathbf{S}_2 \Phi \\ \vdots \\ \mathbf{S}_N \Phi \end{bmatrix} \quad (2.2-8)$$

$$\text{where } \mathbf{S} = [\mathbf{S}_1, \mathbf{S}_2, \dots, \mathbf{S}_N]^T = \begin{bmatrix} S_{1,1} & S_{1,2} & \dots & S_{1,N} \\ S_{2,1} & S_{2,2} & \dots & S_{2,N} \\ \vdots & \vdots & \ddots & \vdots \\ S_{N,1} & S_{N,2} & \dots & S_{N,N} \end{bmatrix},$$

and we can obtain the solution of  $\phi$  by solving the linear system in Eq. (2.2-1).

Additionally, we define  $\mathbf{S}^{ij}$  as the  $\mathbf{S}$  whose given operator is the second-order partial spatial derivatives with respect to  $x_i$  and  $x_j$  in this thesis; that is,  $\zeta\{\cdot\} = \partial^2 / \partial x_i \partial x_j \{\cdot\}$  where  $i, j$  represent the indices of Cartesian spatial dimension number.

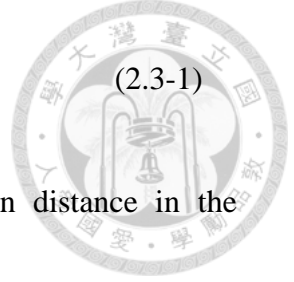
## 2.3 Radial basis function

The radial basis functions (RBFs) have been frequently utilized and applied to approximate scattered data in recent years. By the Euclidean distance  $r$ , the LRBFCM can form the discretization equation. However, there are several types shown in the Table.2.3.1 where the shape parameter is denoted by  $c$ . The decision of appropriate shape parameter is very cumbersome especially in practical engineering problems. We will elucidate that in the following section.

Table.2.3.1. List of commonly-used RBFs

Name of RBFs	Formulation
Multiquadric (MQ)	$\sqrt{r^2+c^2}, c > 0$
Inverse multiquadric (IMQ)	$1/\sqrt{r^2+c^2}, c > 0$
General Multiquadric (GMQ)	$(r^2+c^2)^{1/n}, c > 0 (n=1,3,5...)$
Gaussian (GA)	$\exp(-cr^2), c > 0$
Polyharmonic Splines (PS) of order m in 2D	$r^{2m} \ln(r)$
Polyharmonic Splines (PS) of order m in 3D	$r^{2m-1}$

Franke [32] compared several methods in 1982 from the characteristics, such as accuracy, sensitivity to parameters, timing, storage requirements, and so on. Among the methods, the multiquadric RBF (MQ-RBF), that is Hardy's multiquadric method, is one of the most frequently-used methods due to the characteristics of accuracy and stability in the LRBFCM. Therefore, we adopt the MQ-RBF and use it to form the approximate equations in this thesis. To utilize the radial basis function  $f$  as the MQ-RBF with respect to computation points  $\mathbf{x}$  and  $\mathbf{x}^k$ , the radial basis function can be expressed as



$$f^k = f^k(r) \quad (2.3-1)$$

where  $r = \|\mathbf{x} - \mathbf{x}^k\| = \sqrt{(x_1 - x_1^k)^2 + \dots + (x_d - x_d^k)^2}$  is the Euclidean distance in the Cartesian coordinate system and  $d$  is the number of spatial dimension. The differential formulation in the Cartesian coordinate system is shown in Table.2.3.2.

Table.2.3.2. The differential formulation of the MQ-RBF

	2-dimensional formulation	3-dimensional formulation
$f$	$(r^2 + c^2)^{\frac{1}{2}}$	$(r^2 + c^2)^{\frac{1}{2}}$
$\frac{\partial f}{\partial x_1}$	$\frac{x_1 - x_1^k}{(r^2 + c^2)^{\frac{1}{2}}}$	$\frac{x_1 - x_1^k}{(r^2 + c^2)^{\frac{1}{2}}}$
$\frac{\partial f}{\partial x_2}$	$\frac{x_2 - x_2^k}{(r^2 + c^2)^{\frac{1}{2}}}$	$\frac{x_2 - x_2^k}{(r^2 + c^2)^{\frac{1}{2}}}$
$\frac{\partial f}{\partial x_3}$	0	$\frac{x_3 - x_3^k}{(r^2 + c^2)^{\frac{1}{2}}}$
$\frac{\partial^2 f}{\partial x_1^2}$	$\frac{1}{(r^2 + c^2)^{\frac{1}{2}}} - \frac{(x_1 - x_1^k)^2}{(r^2 + c^2)^{\frac{3}{2}}}$	$\frac{1}{(r^2 + c^2)^{\frac{1}{2}}} - \frac{(x_1 - x_1^k)^2}{(r^2 + c^2)^{\frac{3}{2}}}$
$\frac{\partial^2 f}{\partial x_2^2}$	$\frac{1}{(r^2 + c^2)^{\frac{1}{2}}} - \frac{(x_2 - x_2^k)^2}{(r^2 + c^2)^{\frac{3}{2}}}$	$\frac{1}{(r^2 + c^2)^{\frac{1}{2}}} - \frac{(x_2 - x_2^k)^2}{(r^2 + c^2)^{\frac{3}{2}}}$
$\frac{\partial^2 f}{\partial x_3^2}$	0	$\frac{1}{(r^2 + c^2)^{\frac{1}{2}}} - \frac{(x_3 - x_3^k)^2}{(r^2 + c^2)^{\frac{3}{2}}}$
$\frac{\partial^2 f}{\partial x_1 \partial x_2}$	$-\frac{(x_1 - x_1^k)(x_2 - x_2^k)}{(r^2 + c^2)^{\frac{3}{2}}}$	$-\frac{(x_1 - x_1^k)(x_2 - x_2^k)}{(r^2 + c^2)^{\frac{3}{2}}}$

$\frac{\partial^2 f}{\partial x_1 \partial x_3}$	0	$-\frac{(x_1 - x_1^k)(x_3 - x_3^k)}{(r^2 + c^2)^{\frac{3}{2}}}$
$\frac{\partial^2 f}{\partial x_2 \partial x_3}$	0	$-\frac{(x_2 - x_2^k)(x_3 - x_3^k)}{(r^2 + c^2)^{\frac{3}{2}}}$

## 2.4 Local influence area

The numerical accuracy and stability of LRBFCM are highly dependent on the local influence area. Inappropriate local influence will possibly cause the ill-conditioned resultant interpolation matrix. Therefore, there have been many fashions of selection of local influence area developed to deal with the above problems. The most popular three fashions are the selection of fixed number of the nearest points, the selection of points within the fixed radius, and the cross-shaped selection. Due to the easy implementation, we adopt the selection of fixed number of the nearest points in this research.

First, the selection of fixed number of the nearest points is the easiest and most common selection method due to its characteristic of simple coding. By utilizing this method of selection, we should determine the number of the nearest points with respect to every computation point. To exemplify, the two-dimensional uniform point distribution case is shown in Fig.2.4.1. It is obvious that the selection in the boundary and corner is asymmetric and unbalanced. This phenomenon will become more

significant in the non-uniform point.

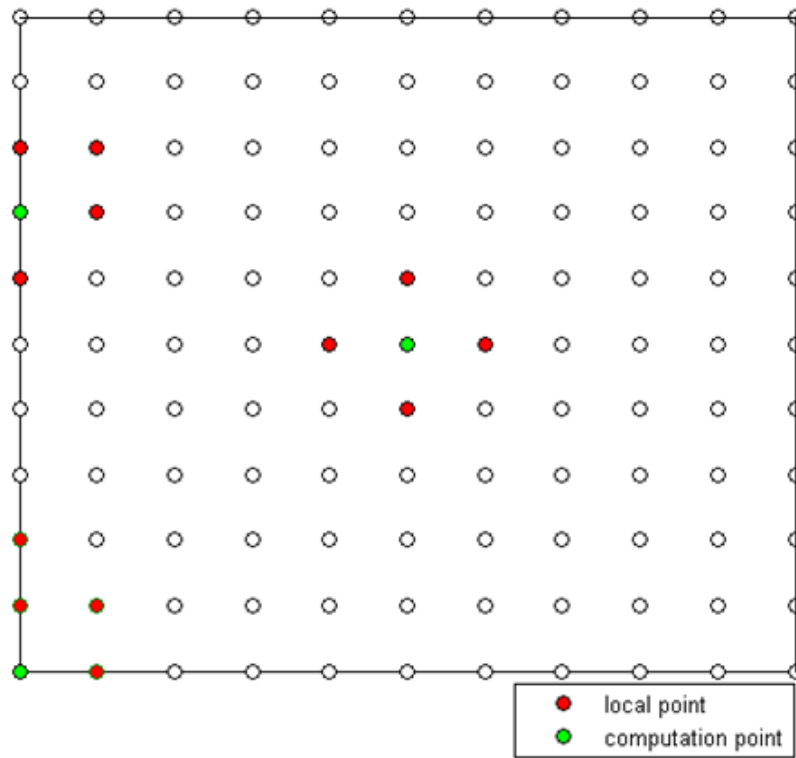


Fig.2.4.1 The number of the nearest points with respect to every computation point by choosing  $NL = 5$  in the two-dimensional uniform point distribution case.

Second, the selection of points within the fixed radius is also a commonly-used method which should be given a radius to determine the local points with respect to every computation point. From Fig.2.4.2, computational inefficiency possibly occurred in the relatively dense region and insufficient local points are illustrated. If the non-uniform point distribution cases or the problems with the much different length scales in three dimensions are applied by the selection of fixed number of the nearest points, this phenomenon will be more significant which increases the opportunity of

occurrence of numerical instability and ill-conditioned matrix.

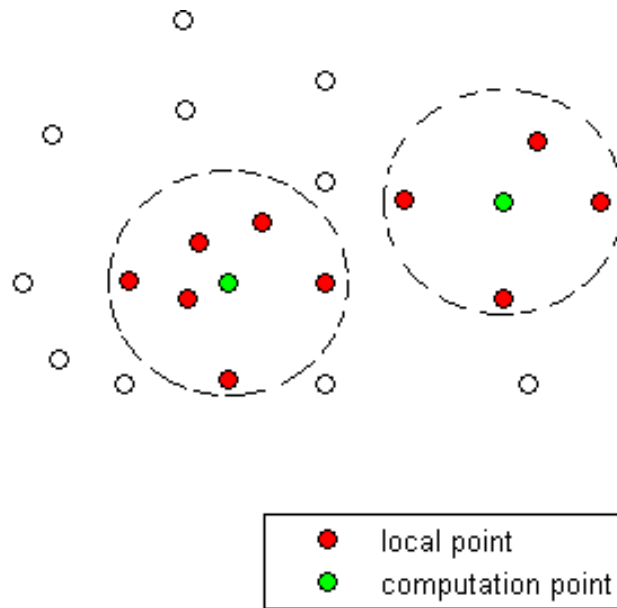


Fig.2.4.2 The selection of points within the fixed radius in the two-dimensional non-uniform point distribution case.

Third, the cross-shaped selection [33] as shown in Fig.2.4.3, which utilizes the provided shape of local influence area and provided number of local points with respect to computation point to determine the local point within each local domain, provides more efficient computation and lowers the opportunity of occurrence of numerical instability and ill-conditioned matrix.



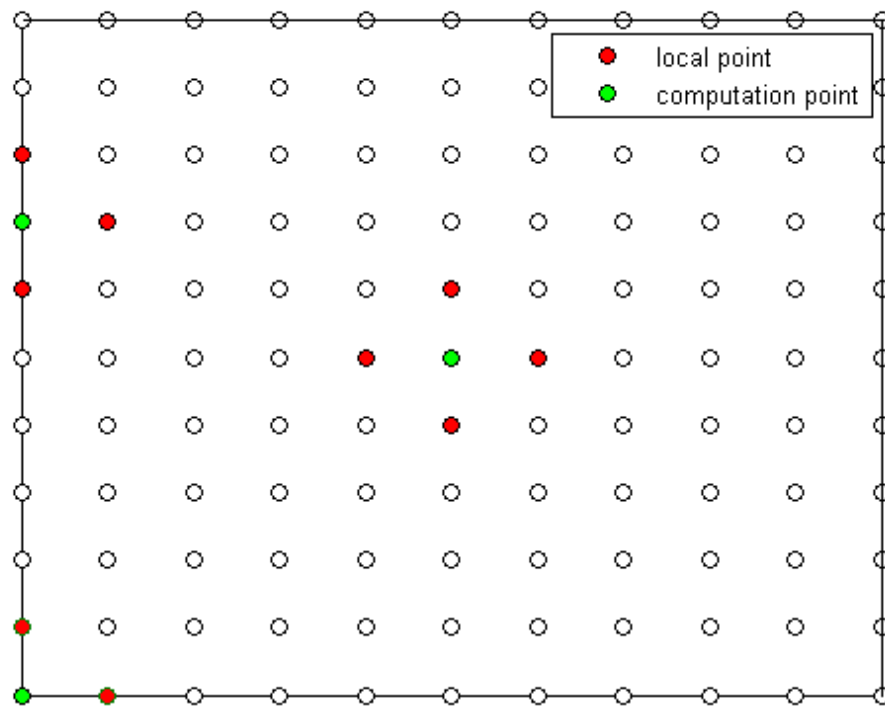


Fig.2.4.3 The cross-shaped selection.

## 2.5 Shape parameter

The decision of optimal shape parameter  $c$  plays a crucial role in the stability and accuracy of the LRBFCM for different numerical applications. It strongly depends on geometry of global domain and types of point distributions.

In general, shape parameter is located on the specific range. If  $c$  is too small, it could result in the singularity; however, if  $c$  is too big, the influence of radius will be decreased by the shape parameter. It is very difficult to determine optimal shape parameter when we deal with the problems which the length scales in three dimensions

are much different. We will introduce and elucidate a normalization technique to assure optimal shape parameter to be in the same order in the next section.



## 2.6 Normalization technique

Many normalization techniques have been developed due to the difficulty of determination of optimal shape parameter. Generally, normalization techniques can be divided by two parts, normalized distance and normalized shape parameter.

### 2.6.1 Normalized distance

One of the most popular normalization techniques is to normalize the distance as

$$r_{i,k,m} = \sqrt{\sum_{d=1}^{Nd} \left( \frac{x_{d,i,k} - x_{d,i,m}}{L_{d,i}} \right)^2} \quad (2.6.1-1)$$

where  $r_{i,k,m}$  is the distance between the collocation points within the local influence area  $\omega_i$ ,  $x_{d,i,k}$  denotes the position of the  $k$ th local point within the local influence area  $\omega_i$  in the  $d$ th dimension,  $Nd$  is the total number of spatial dimension, and the maximum distance between collocation points in all the dimensions within the local influence area  $\omega_i$  is defined as  $L_{d,i}$ .

### 2.6.2 Normalized shape parameter

Another normalization technique is developed in [26] and it is to normalize the given shape parameter  $c$  associated with each local influence area  $\omega_i$  as

$$c_i = c \times L_i, \quad (2.6.2-1)$$

where  $c_i$  is the normalized shape parameter and  $L_i$  is the maximum distance between the computation points within the local influence area  $\omega_i$ . By normalizing the shape parameter, the range of optimal shape parameter could be narrowed.

Due to the efficiency and improvement, we adopt the second normalization technique, normalized shape parameter, for simulation of piezoelectric problems in this thesis. Additionally, there are the cross partial derivative terms in our problems (see Eqs. (4.2-19)-(4.2-23) in Chapter 4), so the local influence must cover more local points rather than local points of cross-shaped selection. As a result, normalization technique of shape parameter is necessary to solve piezoelectric problems.

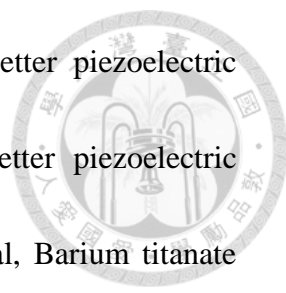
## Chapter 3 Piezoelectricity



### 3.1 Historical overview

The story of the piezoelectric materials starts in 1880, when the Pierre and Jacques Curie discovered [34] that several natural materials, including quartz and Rochelle salt, exhibited a special property. The Curie brothers demonstrated that if the specially prepared materials were imposed a mechanical stress, an electric output was produced. They showed this coupling by measuring the charge induced across electrodes placed on the material when it was imposed an applied mechanical deformation. They defined this effect *the piezoelectric effect*. The name comes from a Greek word for squeeze – *piezein*. Few years later it was demonstrated by Gabriel Lippmann [35] that piezoelectric materials also exhibited the reciprocal property; namely, a mechanical strain was induced when an electric field was applied to the materials.

However, the coupling weak, which means the amount of electrical signal produced by applied mechanical deformation was small, limited the application due to the lack of precision instrumentation. The first engineering application was developed to locate submarines, which is the basis of sonar, until World War I. The piezoelectric materials were widely used in sonar during World War II and developments in electronics also stimulate different uses of piezoelectric materials, such as electronic



oscillators and filters. On account of the increasing need for better piezoelectric materials, the synthetic materials were developed to exhibit better piezoelectric properties. To exemplify, the early synthetic piezoelectric material, Barium titanate ( $\text{BaTiO}_3$ ), is superior to quartz crystals in piezoelectric and thermal properties. In the 1950s and 1960s the most widely used piezoelectric material, lead-zirconate-titanate (PZT), was developed and motivated more applications. Nowadays, piezoelectricity is utilized everywhere. For example, motion and force sensors, the airbag, accelerometers, and atomic force microscopes (AFMs). The application in civil engineering will be presented in section 3.3.

### **3.2 Principles of piezoelectric effect**

The piezoelectric effect can be divided by two types as shown in Fig.3.2.1. The first is the direct piezoelectric effect which depicts piezoelectric materials transform the applied mechanical strain into the electric output. The second is the converse effect which describe mechanical strain energy is produced by an applied electrical potential on piezoelectric materials.

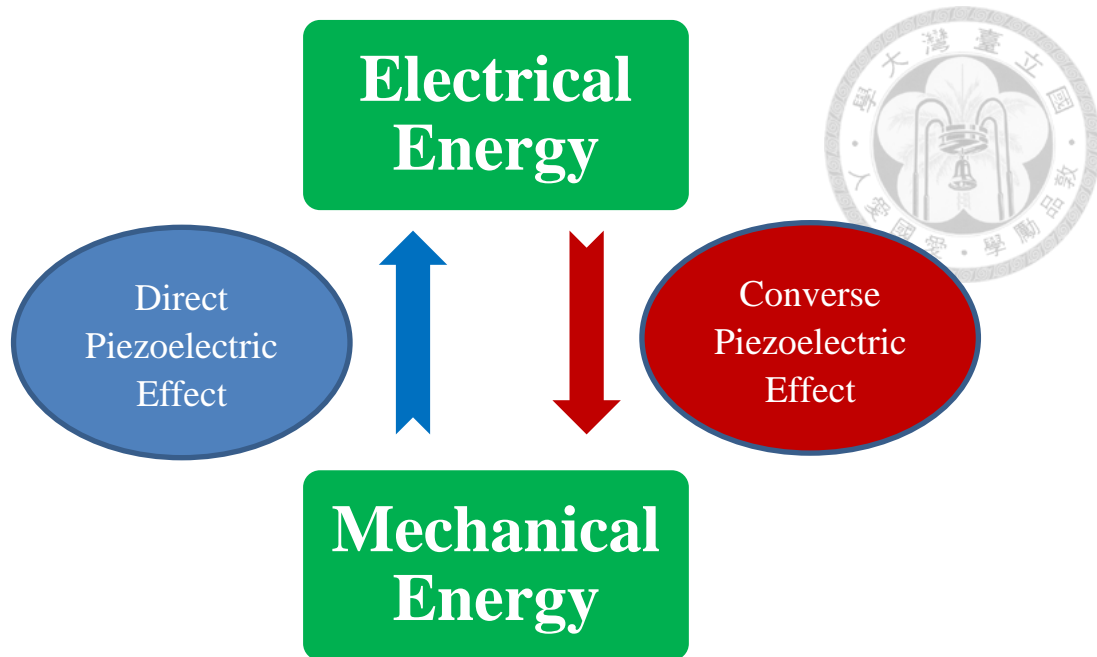


Fig.3.2.1. The illustration of the relations between the energies and the piezoelectric effects.

In general, we will utilize the direct piezoelectric effect to be a sensor and utilize the converse piezoelectric effect to be an actuator. From Fig.3.2.1, if the piezoelectric material generates a positive electric field by the applied tensile stress (see (a)), the applied compressive load will generate a negative electric field (see (b)). Furthermore, the converse piezoelectric effect also exhibits this phenomenon. If the positive electric field is imposed on the piezoelectric material and generates a contraction of the material, an expansion of the material will be generated by the applied negative electric field.

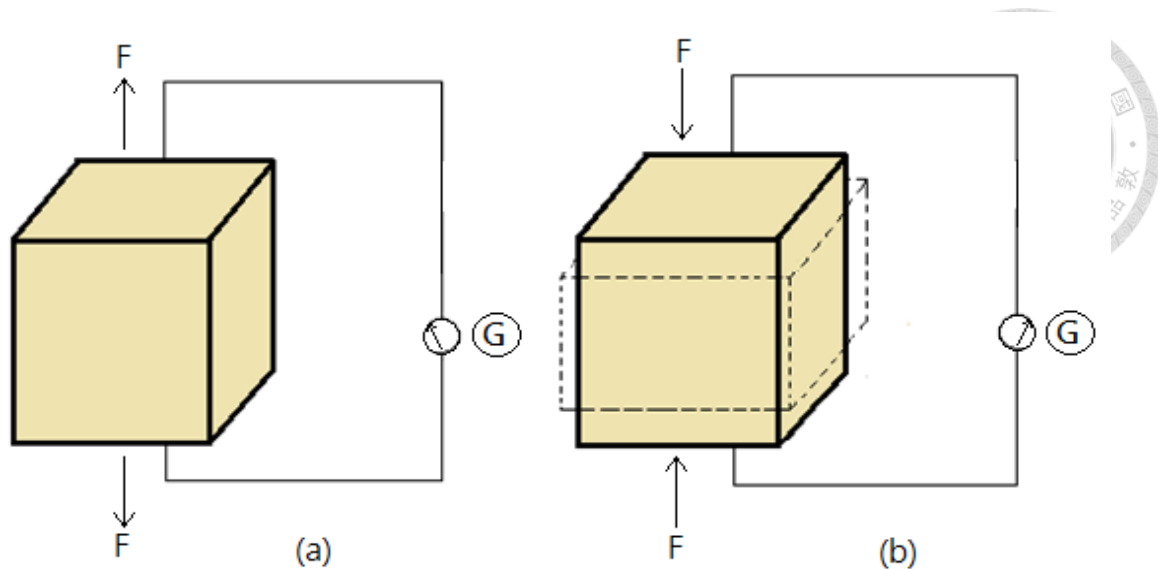
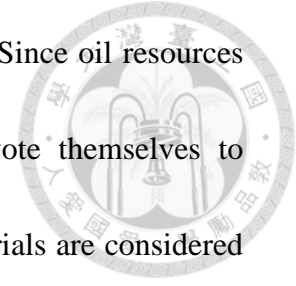


Fig.3.2.1 Configuration of the direct piezoelectric effect. (G: galvanometer)

### 3.3 Applications in civil engineering

In recent decades, there have been many piezoelectric applications in civil engineering due to advances of science and technology. The so-called smart materials, which can be significantly changed by the applied stimuli such as stress or electric output, were presented [36]. This thesis also introduces the related applications of smart materials including piezoelectric materials to civil and mechanical infrastructure systems. Piezoelectric materials have been playing an important role in the vibration control of structures [37]. In addition, piezoelectric materials are also applied [38] in structural damping mechanism by passive electrical circuits, while piezoceramics [39] are used in various forms for active control of structural vibration and are applied in civil structures such as beams and steel frames. The embedded piezoelectric wafer active sensors (PWAS) [40] perform an important function in structural health

monitoring (SHM) by exciting and detecting tuned Lamb waves. Since oil resources have been gradually depleted, more and more researchers devote themselves to alternative technology of power harvesting and piezoelectric materials are considered a feasible and renewable resources. Erturk [41] introduced and analyzed the energy harvesting of piezoelectric materials from moving load excitations and surface strain fluctuations in civil infrastructure system.



### **3.4 Functionally graded materials**

In recent decades, a novel advanced materials, functionally graded materials (FGMs), have been gradually attached importance in various engineering applications. The characteristic of FGMs is that continuous and gradual variation of material properties over the spatial coordinates. The difference of structure between two-layered composites and FGMs is shown in Fig.3.4.1. FGMs have shown advantage of better performance over multilayered composites. In general, conventional multilayered composites suffer from abrupt changes of material properties [42] at the interface between contiguous layers of composites which results in problems such as delamination and large residual thermal stresses. In contrast, FGMs are utilized to reduce the stress concentration and the fracture toughness [43][44].

From the above advantages, the properties of FGMs provide prospect for



applications of piezoelectric materials. The attributes of low thermal expansion coefficient, low dielectric constant, high toughness, high strength, and increase of gradient of the material properties [45] can be applied to extend the lifetime, and improve reliability of piezoelectric structures [46]. In general, the grading variation is defined by power-law, sigmoid, or exponential function. In this work the exponential function is adopted and we will elucidate the definition of grading properties in Eq. (4.2-24).

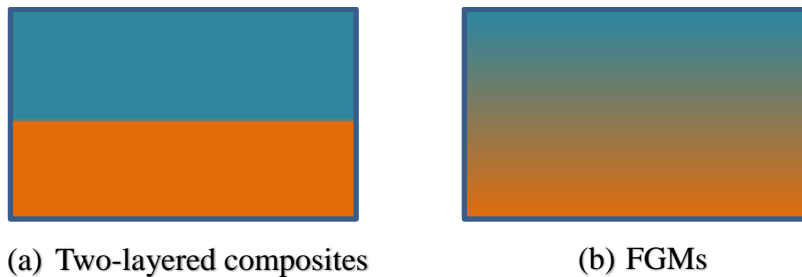
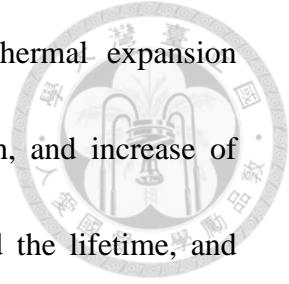


Fig.3.4.1 Configuration of two-layered composites and FGMs.

### 3.5 The constitutive equations of piezoelectric materials

From thermodynamic considerations, the constitutive equations of piezoelectric materials can be categorized into the following four forms [47] with respect to their independent variables:

$\varepsilon - D$  form:

$$\begin{aligned} \sigma &= c^D \varepsilon - kD \\ E &= -k\varepsilon + \beta^e D \end{aligned} \tag{3.5-1}$$

$\sigma - E$  form:

$$\varepsilon = s^E \sigma - dE$$

$$D = d\sigma + h^E E$$



(3.5-2)

$\sigma - D$  form:

$$\varepsilon = s^D \sigma + gD$$

$$E = -g\sigma + \beta^D D$$

(3.5-3)

$\varepsilon - E$  form:

$$\sigma = c^E \varepsilon - eE$$

$$D = e\varepsilon + h^E E$$

(3.5-4)

where  $\sigma$ ,  $\varepsilon$ ,  $D$ , and  $E$  denote the stress, strain, electric displacement, and electric field, respectively. The stiffness constants at a constant electric displacement and a constant electric field are  $c^D$   $c^E$ , respectively. The compliance constants  $s^D$   $s^E$  are at a constant electric displacement and a constant electric field, respectively. The dielectric constants (permittivity) at a constant strain and a constant stress are  $h^E$   $h^\sigma$ , respectively. The impermeability constants  $\beta^E$   $\beta^\sigma$  are at a constant strain and a constant stress, respectively. The constants  $k$ ,  $d$ ,  $g$ , and  $e$  are piezoelectric constants. To exemplify, the  $\sigma - E$  form of the constitutive equation in Eq. (3.5-4) can be rewritten in tensor as



$$\sigma_{ij} = c_{ijkl}^E \varepsilon_{kl} - e_{kij} E_k$$

$$D_i = e_{ikl} \varepsilon_{kl} + h_{ik}^E E_k$$

(3.5-5)

where  $(i, j, k, l = 1, 2, 3)$ .

Then, the above equation can be depicted in the matrix form as:

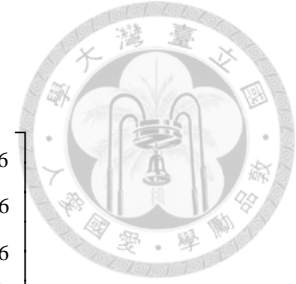
$$\begin{bmatrix} \sigma_{11} \\ \sigma_{22} \\ \sigma_{33} \\ \sigma_{23} \\ \sigma_{13} \\ \sigma_{12} \end{bmatrix} = \begin{bmatrix} c_{11}^E & c_{12}^E & c_{13}^E & c_{14}^E & c_{15}^E & c_{16}^E \\ c_{21}^E & c_{22}^E & c_{23}^E & c_{24}^E & c_{25}^E & c_{26}^E \\ c_{31}^E & c_{32}^E & c_{33}^E & c_{34}^E & c_{35}^E & c_{36}^E \\ c_{41}^E & c_{42}^E & c_{43}^E & c_{44}^E & c_{45}^E & c_{46}^E \\ c_{51}^E & c_{52}^E & c_{53}^E & c_{54}^E & c_{55}^E & c_{56}^E \\ c_{61}^E & c_{62}^E & c_{63}^E & c_{64}^E & c_{65}^E & c_{66}^E \end{bmatrix} \begin{bmatrix} \varepsilon_{11} \\ \varepsilon_{22} \\ \varepsilon_{33} \\ 2\varepsilon_{23} \\ 2\varepsilon_{31} \\ 2\varepsilon_{12} \end{bmatrix} - \begin{bmatrix} e_{11} & e_{21} & e_{31} \\ e_{12} & e_{22} & e_{32} \\ e_{13} & e_{23} & e_{33} \\ e_{14} & e_{24} & e_{34} \\ e_{15} & e_{25} & e_{35} \\ e_{16} & e_{26} & e_{36} \end{bmatrix} \begin{bmatrix} E_1 \\ E_2 \\ E_3 \end{bmatrix}$$

$$\begin{bmatrix} D_1 \\ D_2 \\ D_3 \end{bmatrix} = \begin{bmatrix} e_{11} & e_{12} & e_{13} & e_{14} & e_{15} & e_{16} \\ e_{21} & e_{22} & e_{23} & e_{24} & e_{25} & e_{26} \\ e_{31} & e_{32} & e_{33} & e_{34} & e_{35} & e_{36} \end{bmatrix} \begin{bmatrix} \varepsilon_{11} \\ \varepsilon_{22} \\ \varepsilon_{33} \\ 2\varepsilon_{23} \\ 2\varepsilon_{31} \\ 2\varepsilon_{12} \end{bmatrix} + \begin{bmatrix} h_{11}^E & h_{12}^E & h_{13}^E \\ h_{21}^E & h_{22}^E & h_{23}^E \\ h_{31}^E & h_{32}^E & h_{33}^E \end{bmatrix} \begin{bmatrix} E_1 \\ E_2 \\ E_3 \end{bmatrix} \quad (3.5-6)$$

With different symmetry type of material properties, piezoelectric behavior and the above equations vary.

The analyzed piezoelectric ceramic materials in this thesis exhibit transversely isotropic elastic behavior with hexagonal symmetry of class 6 mm with  $x_3$  as the poling direction and  $x_1 - x_2$  plane as the isotropic plane. Material coefficients in the matrix form of the constitutive equations utilize the Voigt notation to express. For the hexagonal system the principal axis has order six, behaving as a diad axis combined with a triad. The matrix of stiffness constants thus has a form combining the features of

the monoclinic and trigonal systems



$$\begin{array}{l}
 \text{Monoclinic :} \\
 \begin{bmatrix} c_{11} & c_{12} & c_{13} & 0 & 0 & c_{16} \\ c_{12} & c_{11} & c_{13} & 0 & 0 & c_{26} \\ c_{13} & c_{23} & c_{33} & 0 & 0 & c_{36} \\ 0 & 0 & 0 & c_{44} & c_{45} & 0 \\ 0 & 0 & 0 & c_{45} & c_{55} & 0 \\ c_{16} & c_{26} & c_{36} & 0 & 0 & c_{66} \end{bmatrix} \\
 \\
 \text{Tetragonal :} \\
 \begin{bmatrix} c_{11} & c_{12} & c_{13} & c_{14} & -c_{25} & 0 \\ c_{12} & c_{11} & c_{13} & -c_{14} & c_{25} & 0 \\ c_{13} & c_{13} & c_{33} & 0 & 0 & 0 \\ c_{14} & -c_{14} & 0 & c_{44} & 0 & c_{25} \\ -c_{25} & c_{25} & 0 & 0 & c_{44} & c_{14} \\ 0 & 0 & 0 & c_{25} & c_{14} & (c_{11} - c_{12})/2 \end{bmatrix},
 \end{array}$$

giving

$$\text{Hexagonal :} \begin{bmatrix} c_{11} & c_{12} & c_{13} & 0 & 0 & 0 \\ c_{12} & c_{11} & c_{13} & 0 & 0 & 0 \\ c_{13} & c_{13} & c_{33} & 0 & 0 & 0 \\ 0 & 0 & 0 & c_{44} & 0 & 0 \\ 0 & 0 & 0 & 0 & c_{55} & 0 \\ 0 & 0 & 0 & 0 & 0 & (c_{11} - c_{12})/2 \end{bmatrix}.$$

The class 6mm possesses three diad axes which has the same properties as those of the class 2mm and class 6.

$$\begin{array}{l}
 \text{Class 6 :} \\
 \begin{bmatrix} 0 & 0 & 0 & e_{14} & e_{15} & 0 \\ 0 & 0 & 0 & e_{15} & -e_{14} & 0 \\ e_{31} & e_{31} & e_{33} & 0 & 0 & 0 \end{bmatrix} \\
 \\
 \text{Class 2mm :} \\
 \begin{bmatrix} 0 & 0 & 0 & 0 & e_{15} & 0 \\ 0 & 0 & 0 & e_{24} & 0 & 0 \\ e_{31} & e_{32} & e_{33} & 0 & 0 & 0 \end{bmatrix}
 \end{array}$$

Therefore, the matrix of piezoelectric moduli (coefficients) of class 6mm gives

$$\text{Class } 6mm: \begin{bmatrix} 0 & 0 & 0 & 0 & e_{15} & 0 \\ 0 & 0 & 0 & e_{15} & 0 & 0 \\ e_{31} & e_{31} & e_{33} & 0 & 0 & 0 \end{bmatrix}$$



Since the analyzed material is semiconductors, the governing equations have to be supplemented by constitutive equations [48][49] to obtain a unique solution. They express the coupling of the mechanical and electrical fields and electric current fields as

$$\sigma_{ij}(\mathbf{x}, \tau) = c_{ijkl}(\mathbf{x})\varepsilon_{kl}(\mathbf{x}, \tau) - e_{kij}(\mathbf{x})E_k(\mathbf{x}, \tau), \quad (3.5-7)$$

$$D_j(\mathbf{x}, \tau) = e_{jkl}(\mathbf{x})\varepsilon_{kl}(\mathbf{x}, \tau) + h_{jk}(\mathbf{x})E_k(\mathbf{x}, \tau), \quad (3.5-8)$$

$$J_j(\mathbf{x}, \tau) = qM_0\mu_{ij}(\mathbf{x})E_j(\mathbf{x}, \tau) - qd_{ij}(\mathbf{x})M_{,j}(\mathbf{x}, \tau), \quad (3.5-9)$$

where  $c_{ijkl}(\mathbf{x})$ ,  $e_{ijk}(\mathbf{x})$ ,  $h_{ij}(\mathbf{x})$ ,  $\mu_{ij}(\mathbf{x})$  and  $d_{ij}(\mathbf{x})$  are the elastic, piezoelectric, dielectric, electron mobility and carrier diffusion material coefficients, respectively.

$M_0$  is the electron density in the unloaded state. The matrix form of the constitutive equations for the analyzed piezoelectric ceramic materials can be expressed as:

$$\begin{bmatrix} \sigma_{11} \\ \sigma_{22} \\ \sigma_{33} \\ \sigma_{23} \\ \sigma_{13} \\ \sigma_{12} \end{bmatrix} = \begin{bmatrix} c_{11} & c_{12} & c_{13} & 0 & 0 & 0 \\ c_{12} & c_{11} & c_{13} & 0 & 0 & 0 \\ c_{13} & c_{13} & c_{33} & 0 & 0 & 0 \\ 0 & 0 & 0 & c_{44} & 0 & 0 \\ 0 & 0 & 0 & 0 & c_{55} & 0 \\ 0 & 0 & 0 & 0 & 0 & c_{66} \end{bmatrix} \begin{bmatrix} \varepsilon_{11} \\ \varepsilon_{22} \\ \varepsilon_{33} \\ 2\varepsilon_{23} \\ 2\varepsilon_{13} \\ 2\varepsilon_{12} \end{bmatrix} - \begin{bmatrix} 0 & 0 & e_{31} \\ 0 & 0 & e_{31} \\ 0 & 0 & e_{33} \\ 0 & e_{15} & 0 \\ e_{15} & 0 & 0 \\ 0 & 0 & 0 \end{bmatrix} \begin{bmatrix} E_1 \\ E_2 \\ E_3 \end{bmatrix}$$



$$= \mathbf{C}(\mathbf{x}) \begin{bmatrix} \varepsilon_{11} \\ \varepsilon_{22} \\ \varepsilon_{33} \\ 2\varepsilon_{23} \\ 2\varepsilon_{13} \\ 2\varepsilon_{12} \end{bmatrix} - \mathbf{L}(\mathbf{x}) \begin{bmatrix} E_1 \\ E_2 \\ E_3 \end{bmatrix} \quad (3.5-10)$$

$$\begin{bmatrix} D_1 \\ D_2 \\ D_3 \end{bmatrix} = \begin{bmatrix} 0 & 0 & 0 & 0 & e_{15} & 0 \\ 0 & 0 & 0 & e_{15} & 0 & 0 \\ e_{31} & e_{31} & e_{33} & 0 & 0 & 0 \end{bmatrix} \begin{bmatrix} \varepsilon_{11} \\ \varepsilon_{22} \\ \varepsilon_{33} \\ 2\varepsilon_{32} \\ 2\varepsilon_{31} \\ 2\varepsilon_{12} \end{bmatrix} + \begin{bmatrix} h_{11} & 0 & 0 \\ 0 & h_{11} & 0 \\ 0 & 0 & h_{33} \end{bmatrix} \begin{bmatrix} E_1 \\ E_2 \\ E_3 \end{bmatrix}$$

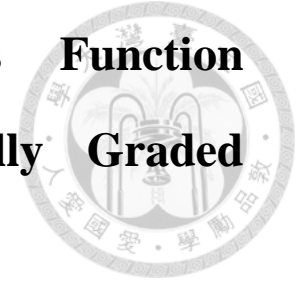
$$= \mathbf{G}(\mathbf{x}) \begin{bmatrix} \varepsilon_{11} \\ \varepsilon_{22} \\ \varepsilon_{33} \\ 2\varepsilon_{32} \\ 2\varepsilon_{31} \\ 2\varepsilon_{12} \end{bmatrix} + \mathbf{H}(\mathbf{x}) \begin{bmatrix} E_1 \\ E_2 \\ E_3 \end{bmatrix} \quad (3.5-11)$$

$$\begin{bmatrix} J_1 \\ J_2 \\ J_3 \end{bmatrix} = qM_0 \begin{bmatrix} \mu_{11} & 0 & 0 \\ 0 & \mu_{22} & 0 \\ 0 & 0 & \mu_{33} \end{bmatrix} \begin{bmatrix} E_1 \\ E_2 \\ E_3 \end{bmatrix} - q \begin{bmatrix} d_{11} & 0 & 0 \\ 0 & d_{22} & 0 \\ 0 & 0 & d_{33} \end{bmatrix} \begin{bmatrix} M_{,1} \\ M_{,2} \\ M_{,3} \end{bmatrix}$$

$$\equiv qM_0 \mathbf{A}(\mathbf{x}) \begin{bmatrix} E_1 \\ E_2 \\ E_3 \end{bmatrix} - q\mathbf{F}(\mathbf{x}) \begin{bmatrix} M_{,1} \\ M_{,2} \\ M_{,3} \end{bmatrix}, \quad (3.5-12)$$

where  $c_{66} = \frac{1}{2}(c_{11} - c_{12})$ .

# Chapter 4 The Local Radial Basis Function Collocation Method for Functionally Graded Piezoelectric Semiconductor

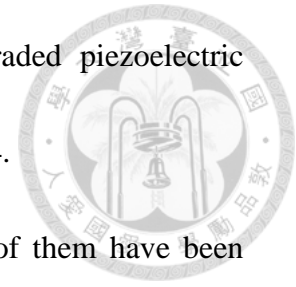


## 4.1 Introduction

Recently, one of smart materials, piezoelectric materials, has received great attention and been utilized in engineering applications. Piezoelectric materials can be applied as transducers, sensors and actuators. Generally, piezoelectric materials can be categorized by two types, non-conducting dielectrics and conductors. However, it is difficult to distinguish between them. Especially, there are more and more synthetic materials. The coupling of the mechanical field, the electrical field and electrical current should be considered [48][49] since the produced electric field and dispersion of elastic waves which result from the space charge. The interaction between mobile charges and a traveling acoustic wave is called an acoustoelectric effect. The above phenomenon is utilized in many acoustoelectric devices [50][51]. Additionally, there are several complicated models of deformable piezoelectric semiconductors in the literature [52][53].

Functionally graded materials (FGMs) have been extensively used in engineering applications. Often, they perform better behaviors than the conventional composites.

There are advanced innovation to manufacture functionally graded piezoelectric materials [54]. The detailed introduction is elucidated in section 3.4.

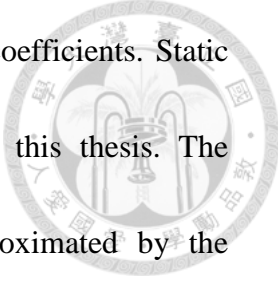


Various meshless methods have been developed and some of them have been proposed to analyze piezoelectric problems [55]-[57]. Continuously nonhomogeneous piezoelectric material properties are considered to analyze non-conducting dielectrics in the literature [58]. Some reviews of meshless methods are presented and analyses of applications in piezoelectric materials are introduced in [59][60]. The element-free Galerkin method (EFG) has been presented [61] to analyze laminated piezoelectric beams; however, the background (shadow) mesh is still required to integrate in this method. The MLPG method has been developed to analyze the three-dimensional elasticity [62], three-dimensional piezoelectricity [63], and three-dimensional axisymmetric continuously non-homogeneous solids [64][65]. Recently, fracture analyses of piezoelectric semiconductors were conducted for anti-plane crack problems [66] and also for thermally induced fracture [67].

The LRBFCM has been utilized to analyze piezoelectric problems [68]. To the best of our knowledge there is no paper on analysis of general three-dimensional functionally graded piezoelectric semiconductor solids using a strong-form meshless method. Therefore, the LRBFCM is proposed to analyze such problems in this thesis.

The three-dimensional analyses are considered no simplification and allows arbitrary





given loading profile, boundary conditions, and grading material coefficients. Static and transient boundary value problems are also investigated in this thesis. The displacements, electric potential, and electron density are approximated by the multiquadric radial basis function (MQ-RBF). The analyzed piezoelectric semiconducting beam is discretized only with points, and no finite element is required. Furthermore, the coupling of the governing equations for mechanical field, electrical field, and current are satisfied in a local strong-form for a set of points. Thus, no integration of the governing equations is required. The essential and natural boundary conditions are also implemented with the collocation of boundary points and their ambient points. If continuous variation of material properties is considered for analyses of functionally graded materials, the conventional numerical methods are difficult to be applied in approximation of governing partial differential equations with non-constant coefficients. By contrast, the LRBFCM has advantages since the independent points. After implementing the spatial RBF approximation, a system of the governing equations for certain point unknowns is obtained in case of transient problems. Then, the system of the governing equations of the second order resulting from the equations of motion is solved by the Houbolt finite-difference scheme [69] as a time-stepping method. Numerical examples are presented for various loading scenarios to analyze the mutual response of mechanical and electrical fields. The influence of material

parameter gradation and initial electron density is also investigated.



## 4.2 Governing equations

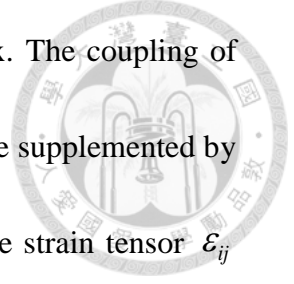
We consider one-carrier piezoelectric semiconductor with continuously nonhomogeneous material (FGM) properties, the electron density  $M_0$  in the unloaded state, and vanishing initial electric field  $E_0$ . In addition, we consider a general variation of material properties with Cartesian coordinates. Since the physical dimension of the device is generally smaller than the electromagnetic wavelength, the quasi-static theory of electromagnetism for the first Maxwell equation is assumed. The phenomenon is expressed by the following governing equations, the balance of momentum, Gauss's law, and conservation of charge [48]

$$\sigma_{ij,j}(\mathbf{x}, \tau) = \rho \ddot{u}_i(\mathbf{x}, \tau), \quad (4.2-1)$$

$$D_{i,i}(\mathbf{x}, \tau) = qM(\mathbf{x}, \tau), \quad (4.2-2)$$

$$q\dot{M}(\mathbf{x}, \tau) + J_{i,i}(\mathbf{x}, \tau) = 0, \quad (4.2-3)$$

where  $\ddot{u}_i$ ,  $\sigma_{ij}$ ,  $D_i$ , and  $q$  are the acceleration of elastic displacements, stress tensor, electric displacement field, and electric charge of electron, respectively. The electron density and electric current are depicted, respectively, by the symbols  $M$  and  $J_i$ .  $\rho$  denotes the mass density. A comma followed by an index denotes



derivative with respect to the coordinate associated with the index. The coupling of mechanical fields, electrical field, and electric current field has to be supplemented by the constitutive equations Eqs. (3.5.10)-(3.5.12) in section 3.5. The strain tensor  $\varepsilon_{ij}$  related to the displacements  $u_i$  and the electric field vector  $E_j$  related to the electric potential  $\phi$  can be expressed by

$$\varepsilon_{ij} = \frac{1}{2}(u_{i,j} + u_{j,i}), \quad (4.2-7)$$

$$E_j = -\phi_{,j}. \quad (4.2-8)$$

Substituting Eqs. (3.5.10)-(3.5.12) into the governing equations Eqs. (4.2-1)-(4.2-3), we obtain the governing equations for the primary fields, displacements, electric potential, and current charge density, and get the system of partial differential equations.

$$\begin{aligned} & c_{11}(\mathbf{x})u_{1,11}(\mathbf{x}, \tau) + \frac{1}{2}(c_{11}(\mathbf{x}) - c_{12}(\mathbf{x}))u_{1,22}(\mathbf{x}, \tau) + \frac{1}{2}(c_{11}(\mathbf{x}) + c_{12}(\mathbf{x}))u_{2,12}(\mathbf{x}, \tau) \\ & + (c_{13}(\mathbf{x}) + c_{55}(\mathbf{x}))u_{3,13}(\mathbf{x}, \tau) + c_{55}(\mathbf{x})u_{1,33}(\mathbf{x}, \tau) + c_{11,1}(\mathbf{x})u_{1,1}(\mathbf{x}, \tau) + c_{12,1}(\mathbf{x})u_{2,2}(\mathbf{x}, \tau) \\ & + c_{13,1}(\mathbf{x})u_{3,3}(\mathbf{x}, \tau) + \frac{1}{2}(c_{11,2}(\mathbf{x}) - c_{12,2}(\mathbf{x}))(u_{1,2}(\mathbf{x}, \tau) + u_{2,1}(\mathbf{x}, \tau)) \\ & + c_{55,3}(\mathbf{x})(u_{1,3}(\mathbf{x}, \tau) + u_{3,1}(\mathbf{x}, \tau)) + (e_{31}(\mathbf{x}) + e_{15}(\mathbf{x}))\phi_{,13}(\mathbf{x}, \tau) + e_{31,1}(\mathbf{x})\phi_{,3}(\mathbf{x}, \tau) \\ & + e_{15,3}(\mathbf{x})\phi_{,1}(\mathbf{x}, \tau) = \rho\ddot{u}_1(\mathbf{x}, \tau), \end{aligned} \quad (4.2-9)$$

$$\begin{aligned} & c_{11}(\mathbf{x})u_{2,22}(\mathbf{x}, \tau) + \frac{1}{2}(c_{11}(\mathbf{x}) - c_{12}(\mathbf{x}))u_{2,11}(\mathbf{x}, \tau) + \frac{1}{2}(c_{11}(\mathbf{x}) + c_{12}(\mathbf{x}))u_{1,21}(\mathbf{x}, \tau) \\ & + (c_{13}(\mathbf{x}) + c_{44}(\mathbf{x}))u_{3,32}(\mathbf{x}, \tau) + c_{44}(\mathbf{x})u_{2,33}(\mathbf{x}, \tau) \end{aligned}$$

$$\begin{aligned}
& + \frac{1}{2} (c_{11,1}(\mathbf{x}) - c_{12,1}(\mathbf{x})) (u_{1,2}(\mathbf{x}, \tau) + u_{2,1}(\mathbf{x}, \tau)) + c_{44,3}(\mathbf{x}) (u_{2,3}(\mathbf{x}, \tau) + u_{3,2}(\mathbf{x}, \tau)) \\
& + c_{12,2}(\mathbf{x}) u_{1,1}(\mathbf{x}, \tau) + c_{11,2}(\mathbf{x}) u_{2,2}(\mathbf{x}, \tau) + c_{13,2}(\mathbf{x}) u_{3,3}(\mathbf{x}, \tau) \\
& + (e_{31}(\mathbf{x}) + e_{15}(\mathbf{x})) \phi_{,23}(\mathbf{x}, \tau) + e_{31,2}(\mathbf{x}) \phi_{,3}(\mathbf{x}, \tau) + e_{15,3}(\mathbf{x}) \phi_{,2}(\mathbf{x}, \tau) = \rho \ddot{u}_2(\mathbf{x}, \tau),
\end{aligned} \tag{4.2-10}$$

$$\begin{aligned}
& c_{55}(\mathbf{x}) u_{3,11}(\mathbf{x}, \tau) + c_{44}(\mathbf{x}) u_{3,22}(\mathbf{x}, \tau) + c_{33}(\mathbf{x}) u_{3,33}(\mathbf{x}, \tau) + (c_{55}(\mathbf{x}) + c_{13}(\mathbf{x})) u_{1,13}(\mathbf{x}, \tau) \\
& + (c_{44}(\mathbf{x}) + c_{13}(\mathbf{x})) u_{2,32}(\mathbf{x}, \tau) + c_{13,3}(\mathbf{x}) (u_{1,1}(\mathbf{x}, \tau) + u_{2,2}(\mathbf{x}, \tau)) + c_{33,3}(\mathbf{x}) u_{3,3}(\mathbf{x}, \tau) \\
& + c_{55,1}(\mathbf{x}) (u_{1,3}(\mathbf{x}, \tau) + u_{3,1}(\mathbf{x}, \tau)) + c_{44,2}(\mathbf{x}) (u_{2,3}(\mathbf{x}, \tau) + u_{3,2}(\mathbf{x}, \tau)) \\
& + e_{15}(\mathbf{x}) (\phi_{,11}(\mathbf{x}, \tau) + \phi_{,22}(\mathbf{x}, \tau)) + e_{33}(\mathbf{x}) \phi_{,33}(\mathbf{x}, \tau) \\
& + e_{15,1}(\mathbf{x}) \phi_{,1}(\mathbf{x}, \tau) + e_{15,2}(\mathbf{x}) \phi_{,2}(\mathbf{x}, \tau) + e_{33,3}(\mathbf{x}) \phi_{,3}(\mathbf{x}, \tau) = \rho \ddot{u}_3(\mathbf{x}, \tau),
\end{aligned} \tag{4.2-11}$$

$$\begin{aligned}
& e_{15}(\mathbf{x}) (u_{3,11}(\mathbf{x}, \tau) + u_{3,22}(\mathbf{x}, \tau)) + e_{33}(\mathbf{x}) u_{3,33}(\mathbf{x}, \tau) \\
& + (e_{15}(\mathbf{x}) + e_{31}(\mathbf{x})) (u_{1,31}(\mathbf{x}, \tau) + u_{2,32}(\mathbf{x}, \tau)) + e_{15,1}(\mathbf{x}) (u_{1,3}(\mathbf{x}, \tau) + u_{3,1}(\mathbf{x}, \tau)) \\
& + e_{15,2}(\mathbf{x}) (u_{2,3}(\mathbf{x}, \tau) + u_{3,2}(\mathbf{x}, \tau)) + e_{31,3}(\mathbf{x}) (u_{1,1}(\mathbf{x}, \tau) + u_{2,2}(\mathbf{x}, \tau)) \\
& + e_{33,3}(\mathbf{x}) u_{3,3}(\mathbf{x}, \tau) - h_{11} \phi_{,11}(\mathbf{x}, \tau) - h_{22} \phi_{,22}(\mathbf{x}, \tau) - h_{33} \phi_{,33}(\mathbf{x}, \tau) \\
& - h_{11,1}(\mathbf{x}) \phi_{,1}(\mathbf{x}, \tau) - h_{22,2}(\mathbf{x}) \phi_{,2}(\mathbf{x}, \tau) - h_{33,3}(\mathbf{x}) \phi_{,3}(\mathbf{x}, \tau) - qM(\mathbf{x}, \tau) = 0,
\end{aligned} \tag{4.2-12}$$

$$\begin{aligned}
& M_0 (\mu_{11}(\mathbf{x}) \phi_{,11}(\mathbf{x}, \tau) + \mu_{22}(\mathbf{x}) \phi_{,22}(\mathbf{x}, \tau) + \mu_{33}(\mathbf{x}) \phi_{,33}(\mathbf{x}, \tau)) \\
& + M_0 (\mu_{11,1}(\mathbf{x}) \phi_{,1}(\mathbf{x}, \tau) + \mu_{22,2}(\mathbf{x}) \phi_{,2}(\mathbf{x}, \tau) + \mu_{33,3}(\mathbf{x}) \phi_{,3}(\mathbf{x}, \tau))
\end{aligned}$$

$$\begin{aligned}
& + (d_{11}(\mathbf{x})M_{,11}(\mathbf{x}, \tau) + d_{22}(\mathbf{x})M_{,22}(\mathbf{x}, \tau) + d_{33}(\mathbf{x})M_{,33}(\mathbf{x}, \tau)) \\
& + d_{11,1}(\mathbf{x})M_{,1}(\mathbf{x}, \tau) + d_{22,2}(\mathbf{x})M_{,2}(\mathbf{x}, \tau) + d_{33,3}(\mathbf{x})M_{,3}(\mathbf{x}, \tau) = \dot{M}(\mathbf{x}, \tau),
\end{aligned} \tag{4.2-13}$$

The above system of PDEs can be simplified due to the homogeneous material properties as:

$$\begin{aligned}
& c_{11}u_{1,11}(\mathbf{x}, \tau) + \frac{1}{2}(c_{11} - c_{12})u_{1,22}(\mathbf{x}, \tau) + \frac{1}{2}(c_{11} + c_{12})u_{2,12}(\mathbf{x}, \tau) \\
& + (c_{13} + c_{55})u_{3,13}(\mathbf{x}, \tau) + c_{55}u_{1,33}(\mathbf{x}, \tau) + (e_{31} + e_{15})\phi_{,13}(\mathbf{x}, \tau) = \rho\ddot{u}_1(\mathbf{x}, \tau),
\end{aligned} \tag{4.2-14}$$

$$\begin{aligned}
& c_{11}u_{2,22}(\mathbf{x}, \tau) + \frac{1}{2}(c_{11} - c_{12})u_{2,11}(\mathbf{x}, \tau) + \frac{1}{2}(c_{11} + c_{12})u_{1,21}(\mathbf{x}, \tau) \\
& + (c_{13} + c_{44})u_{3,32}(\mathbf{x}, \tau) + c_{44}u_{2,33}(\mathbf{x}, \tau) + (e_{31} + e_{15})\phi_{,23}(\mathbf{x}, \tau) = \rho\ddot{u}_2(\mathbf{x}, \tau),
\end{aligned} \tag{4.2-15}$$

$$\begin{aligned}
& c_{55}u_{3,11}(\mathbf{x}, \tau) + c_{44}u_{3,22}(\mathbf{x}, \tau) + c_{33}u_{3,33}(\mathbf{x}, \tau) + (c_{55} + c_{13})u_{1,13}(\mathbf{x}, \tau) \\
& + (c_{44} + c_{13})u_{2,32}(\mathbf{x}, \tau) + e_{15}(\phi_{,11}(\mathbf{x}, \tau) + \phi_{,22}(\mathbf{x}, \tau)) + e_{33}\phi_{,33}(\mathbf{x}, \tau) = \rho\ddot{u}_3(\mathbf{x}, \tau),
\end{aligned} \tag{4.2-16}$$

$$\begin{aligned}
& e_{15}(u_{3,11}(\mathbf{x}, \tau) + u_{3,22}(\mathbf{x}, \tau)) + e_{33}u_{3,33}(\mathbf{x}, \tau) + (e_{15} + e_{31})(u_{1,31}(\mathbf{x}, \tau) + u_{2,32}(\mathbf{x}, \tau)) \\
& - h_{11}\phi_{,11}(\mathbf{x}, \tau) - h_{22}\phi_{,22}(\mathbf{x}, \tau) - h_{33}\phi_{,33}(\mathbf{x}, \tau) - qM(\mathbf{x}, \tau) = 0,
\end{aligned} \tag{4.2-17}$$

$$M_0(\mu_{11}\phi_{,11}(\mathbf{x}, \tau) + \mu_{22}\phi_{,22}(\mathbf{x}, \tau) + \mu_{33}\phi_{,33}(\mathbf{x}, \tau)) \tag{4.2-18}$$

$$+(d_{11}M_{,11}(\mathbf{x}, \tau) + d_{22}M_{,22}(\mathbf{x}, \tau) + d_{33}M_{,33}(\mathbf{x}, \tau)) = \dot{M}(\mathbf{x}, \tau),$$



In order to approximate the unknown variables by the LRBFCM, we rearrange the

above governing equation for convenience as follows:

$$\begin{aligned} & \left[ c_{11} \frac{\partial^2}{\partial x_1^2} + c_{66} \frac{\partial^2}{\partial x_2^2} + c_{55} \frac{\partial^2}{\partial x_3^2} \right] u_1 + \left[ (c_{12} + c_{66}) \frac{\partial^2}{\partial x_1 \partial x_2} \right] u_2 \\ & + \left[ (c_{13} + c_{55}) \frac{\partial^2}{\partial x_1 \partial x_3} \right] u_3 + \left[ (e_{31} + e_{15}) \frac{\partial^2}{\partial x_1 \partial x_3} \right] \phi = \rho \ddot{u}_1, \end{aligned} \quad (4.2-19)$$

$$\begin{aligned} & \left[ (c_{12} + c_{66}) \frac{\partial^2}{\partial x_1 \partial x_2} \right] u_1 + \left[ c_{66} \frac{\partial^2}{\partial x_1^2} + c_{11} \frac{\partial^2}{\partial x_2^2} + c_{44} \frac{\partial^2}{\partial x_3^2} \right] u_2 \\ & + \left[ (c_{13} + c_{44}) \frac{\partial^2}{\partial x_2 \partial x_3} \right] u_3 + \left[ (e_{31} + e_{15}) \frac{\partial^2}{\partial x_2 \partial x_3} \right] \phi = \rho \ddot{u}_2, \end{aligned} \quad (4.2-20)$$

$$\begin{aligned} & \left[ (c_{13} + c_{55}) \frac{\partial^2}{\partial x_1 \partial x_3} \right] u_1 + \left[ (c_{44} + c_{13}) \frac{\partial^2}{\partial x_2 \partial x_3} \right] u_2 \\ & + \left[ c_{55} \frac{\partial^2}{\partial x_1^2} + c_{44} \frac{\partial^2}{\partial x_2^2} + c_{33} \frac{\partial^2}{\partial x_3^2} \right] u_3 + \left[ e_{15} \left( \frac{\partial^2}{\partial x_1^2} + \frac{\partial^2}{\partial x_2^2} \right) + e_{33} \frac{\partial^2}{\partial x_3^2} \right] \phi = \rho \ddot{u}_3, \end{aligned} \quad (4.2-21)$$

$$\begin{aligned} & \left[ (e_{15} + e_{31}) \frac{\partial^2}{\partial x_1 \partial x_3} \right] u_1 + \left[ (e_{15} + e_{31}) \frac{\partial^2}{\partial x_2 \partial x_3} \right] u_2 \end{aligned} \quad (4.2-22)$$

$$+ \left[ e_{15} \left( \frac{\partial^2}{\partial x_1^2} + \frac{\partial^2}{\partial x_2^2} \right) + e_{33} \frac{\partial^2}{\partial x_3^2} \right] u_3 + \left[ -h_{11} \frac{\partial^2}{\partial x_1^2} - h_{11} \frac{\partial^2}{\partial x_2^2} - h_{33} \frac{\partial^2}{\partial x_3^2} \right] \phi - qM = 0,$$



$$M_0 \left[ \mu_{11} \frac{\partial^2}{\partial x_1^2} + \mu_{22} \frac{\partial^2}{\partial x_2^2} + \mu_{33} \frac{\partial^2}{\partial x_3^2} \right] \phi + \left[ d_{11} \frac{\partial^2}{\partial x_1^2} + d_{22} \frac{\partial^2}{\partial x_2^2} + d_{33} \frac{\partial^2}{\partial x_3^2} \right] M = \dot{M}. \quad (4.2-23)$$

For problems of FGMs, the above material coefficients are dependent on the spatial coordinates. One can prescribe an exponential variation of material parameters as

$$P(x_3) = P^{(0)} e^{\delta x_3/h}, \quad (4.2-24)$$

where  $P^{(0)}$  and  $h$  denotes the material property of the elastic, piezoelectric, dielectric and coefficients at  $x_3 = 0$  and beam height, respectively. The grading parameter with respect to the elastic, piezoelectric, dielectric and coefficients is  $\delta$ .

## 4.3 Boundary conditions and initial conditions

### 4.3.1 Boundary conditions

The boundary conditions for the mechanical fields are considered in Eq. (4.3-1).

$$\begin{aligned} u_i(\mathbf{x}, \tau) &= \tilde{u}_i(\mathbf{x}, \tau) && \text{on } \Gamma_u, \\ t_i(\mathbf{x}, \tau) &\equiv \sigma_{ij} n_j = \tilde{t}_i(\mathbf{x}, \tau) && \text{on } \Gamma_t, \Gamma = \Gamma_u \cup \Gamma_t, \end{aligned} \quad (4.3-1)$$

where  $n_j$  is the unit vector normal to the boundary,  $t_i$  denotes the traction vector which is the force per unit area acting on a surface, the given value prescribed on the boundary for displacement, and traction are denoted by  $\tilde{u}_i$  and  $\tilde{t}_i$ , respectively. For the

electrical fields, we assume

$$\begin{aligned} \phi(\mathbf{x}, \tau) &= \tilde{\phi}(\mathbf{x}, \tau) & \text{on } \Gamma_p \\ Q(\mathbf{x}, \tau) &\equiv D_i(\mathbf{x}, \tau)n_i(\mathbf{x}) = \tilde{Q}(\mathbf{x}, \tau) & \text{on } \Gamma_q, \Gamma = \Gamma_p \cup \Gamma_q, \end{aligned} \quad (4.3-2)$$



where  $Q$ ,  $\tilde{\phi}$ , and  $\tilde{Q}$  are the surface density of the free charge, the given values prescribed on the boundary for electric potential, and for surface density of the free charge, respectively. Then for electric charge mobility, the following boundary conditions are considered as

$$\begin{aligned} M(\mathbf{x}, \tau) &= \tilde{M}(\mathbf{x}, \tau) & \text{on } \Gamma_a, \\ S(\mathbf{x}, \tau) &\equiv J_i(\mathbf{x}, \tau)n_i(\mathbf{x}) = \tilde{S}(\mathbf{x}, \tau) & \text{on } \Gamma_b, \Gamma = \Gamma_a \cup \Gamma_b, \end{aligned} \quad (4.3-3)$$

where the electric current flux, the given values prescribed on the boundary for electron density, and for electric current flux are, respectively, represented by  $S$ ,  $\tilde{M}$ , and  $\tilde{S}$ . Additionally,  $\Gamma_u$  is the part of the global boundary  $\Gamma$  with prescribed displacements, while the traction vector, electric potential, surface density of the free charge, electron density, and the electric current flux are applied on  $\Gamma_t$ ,  $\Gamma_p$ ,  $\Gamma_q$ ,  $\Gamma_a$ , and  $\Gamma_b$ , respectively.

In order to apply to the LRBFCM, we substitute the compact matrix form for the constitutive equations in Eqs. (3.5-10)-(3.5-12) into the boundary conditions in Eqs. (4.3-1)- (4.3-3). We obtain Eqs. (4.3-5)-(4.3-6).





$$u_i(\mathbf{x}, \tau) = \tilde{u}_i(\mathbf{x}, \tau)$$

on  $\Gamma_u$ ,

$$t_1 = \left[ c_{11}n_1 \frac{\partial}{\partial x_1} + c_{66}n_2 \frac{\partial}{\partial x_2} + c_{55}n_3 \frac{\partial}{\partial x_3} \right] u_1 + \left[ c_{12}n_1 \frac{\partial}{\partial x_2} + c_{66}n_2 \frac{\partial}{\partial x_1} \right] u_2 + \left[ c_{13}n_1 \frac{\partial}{\partial x_3} + c_{55}n_3 \frac{\partial}{\partial x_1} \right] u_3 + \left[ e_{31}n_1 \frac{\partial}{\partial x_1} + e_{15}n_3 \frac{\partial}{\partial x_1} \right] \phi = \tilde{t}_1$$

$$t_2 = \left[ c_{66}n_1 \frac{\partial}{\partial x_2} + c_{12}n_2 \frac{\partial}{\partial x_1} \right] u_1 + \left[ c_{66}n_1 \frac{\partial}{\partial x_1} + c_{11}n_2 \frac{\partial}{\partial x_2} + c_{44}n_3 \frac{\partial}{\partial x_3} \right] u_2 + \left[ c_{13}n_2 \frac{\partial}{\partial x_3} + c_{44}n_3 \frac{\partial}{\partial x_2} \right] u_3 + \left[ e_{31}n_2 \frac{\partial}{\partial x_3} + e_{15}n_3 \frac{\partial}{\partial x_2} \right] \phi = \tilde{t}_2$$

$$t_3 = \left[ c_{55}n_1 \frac{\partial}{\partial x_3} + c_{13}n_3 \frac{\partial}{\partial x_1} \right] u_1 + \left[ c_{44}n_2 \frac{\partial}{\partial x_3} + c_{13}n_3 \frac{\partial}{\partial x_2} \right] u_2 + \left[ c_{55}n_1 \frac{\partial}{\partial x_1} + c_{44}n_2 \frac{\partial}{\partial x_2} + c_{33}n_3 \frac{\partial}{\partial x_3} \right] u_3 + \left[ e_{15}n_1 \frac{\partial}{\partial x_1} + e_{15}n_2 \frac{\partial}{\partial x_2} + e_{33}n_3 \frac{\partial}{\partial x_3} \right] \phi = \tilde{t}_3$$

on  $\Gamma_t$ ,  $\Gamma = \Gamma_u \cup \Gamma_t$ , (4.3-4)



$$\phi(\mathbf{x}, \tau) = \tilde{\phi}(\mathbf{x}, \tau)$$

on  $\Gamma_p$

$$Q = \left[ e_{15}n_1 \frac{\partial}{\partial x_3} + e_{31}n_3 \frac{\partial}{\partial x_1} \right] u_1 + \left[ e_{15}n_2 \frac{\partial}{\partial x_3} + e_{31}n_3 \frac{\partial}{\partial x_2} \right] u_2 + \left[ e_{15}n_1 \frac{\partial}{\partial x_1} + e_{15}n_2 \frac{\partial}{\partial x_2} + e_{33}n_3 \frac{\partial}{\partial x_3} \right] u_3$$

$$+ \left[ -h_{11}n_1 \frac{\partial}{\partial x_1} - h_{22}n_2 \frac{\partial}{\partial x_2} - h_{33}n_3 \frac{\partial}{\partial x_3} \right] \phi = \tilde{Q}$$

on  $\Gamma_q, \Gamma = \Gamma_p \cup \Gamma_q,$

(4.3-5)

$$M(\mathbf{x}, \tau) = \tilde{M}(\mathbf{x}, \tau)$$

on  $\Gamma_a,$

$$S = M_0 \left[ \mu_{11}n_1 \frac{\partial}{\partial x_1} + \mu_{22}n_2 \frac{\partial}{\partial x_2} + \mu_{33}n_3 \frac{\partial}{\partial x_3} \right] \phi + \left[ d_{11}n_1 \frac{\partial}{\partial x_1} + d_{22}n_2 \frac{\partial}{\partial x_2} + d_{33}n_3 \frac{\partial}{\partial x_3} \right] M = \tilde{S}$$

on  $\Gamma_b, \Gamma = \Gamma_a \cup \Gamma_b,$

(4.3-6)



### 4.3.2 Initial conditions

The initial conditions for the mechanical displacements, electric potential, and the current charge density are assumed as

$$u_i(\mathbf{x}, \tau)|_{\tau=0} = u_i(\mathbf{x}, 0)$$

$$\phi(\mathbf{x}, \tau)|_{\tau=0} = \phi(\mathbf{x}, 0)$$

$$M(\mathbf{x}, \tau)|_{\tau=0} = M(\mathbf{x}, 0) \quad \text{in} \quad \Omega \quad (4.3-7)$$

## 4.4 Numerical solution by the local radial basis function collocation method

By the discussions in chapter 4, the implementation is introduced in this section.

### 4.4.1 The transient analysis

By the LRBFCM, we recall the chapter 2 and approximate the variables in Eqs. (4.3-11)-(4.3-15) as

$$u_1(\mathbf{x}, \tau) = \sum_{k=1}^{NL} \alpha_{i,k}^{u_1} f(\|\mathbf{x} - \mathbf{x}_{i,k}\|) = \mathbf{F}_i(\mathbf{x}) \mathbf{a}_i^{u_1}, \quad \mathbf{x}_{i,k} \in \omega_i \quad (4.4-1)$$

$$u_2(\mathbf{x}, \tau) = \sum_{k=1}^{NL} \alpha_{i,k}^{u_2} f(\|\mathbf{x} - \mathbf{x}_{i,k}\|) = \mathbf{F}_i(\mathbf{x}) \mathbf{a}_i^{u_2}, \quad \mathbf{x}_{i,k} \in \omega_i \quad (4.4-2)$$

$$u_3(\mathbf{x}, \tau) = \sum_{k=1}^{NL} \alpha_{i,k}^{u_3} f(\|\mathbf{x} - \mathbf{x}_{i,k}\|) = \mathbf{F}_i(\mathbf{x}) \mathbf{a}_i^{u_3}, \quad \mathbf{x}_{i,k} \in \omega_i \quad (4.4-3)$$



$$\phi(\mathbf{x}, \tau) = \sum_{k=1}^{NL} \alpha_{i,k}^{\phi} f(\|\mathbf{x} - \mathbf{x}_{i,k}\|) = \mathbf{F}_i(\mathbf{x}) \boldsymbol{\alpha}_i^{\phi}, \mathbf{x}_{i,k} \in \omega_i \quad (4.4-4)$$

$$M(\mathbf{x}, \tau) = \sum_{k=1}^{NL} \alpha_{i,k}^M f(\|\mathbf{x} - \mathbf{x}_{i,k}\|) = \mathbf{F}_i(\mathbf{x}) \boldsymbol{\alpha}_i^M, \mathbf{x}_{i,k} \in \omega_i \quad (4.4-5)$$

where all the computation points are within the local influence area  $\omega_i$  with respect to each computation point  $\mathbf{x}_i$ . In addition, we approximate the second-order partial derivative terms with respect to time by the Houbolt finite-difference scheme [69]. The acceleration of elastic displacement  $\ddot{u}_i$  in the  $x_i$  dimension can be defined as

$$\ddot{u}_1(\mathbf{x}, \tau + \Delta\tau) \cong \frac{2u_1(\mathbf{x}, \tau + \Delta\tau) - 5u_1(\mathbf{x}, \tau) + 4u_1(\mathbf{x}, \tau - \Delta\tau) - u_1(\mathbf{x}, \tau - 2\Delta\tau)}{\Delta\tau^2} \quad (4.4-6)$$

and the first-order temporal partial derivative term,  $\dot{M}$ , can be approximated as

$$\dot{M}(\mathbf{x}, \tau + \Delta\tau) \cong \frac{M(\mathbf{x}, \tau + \Delta\tau) - M(\mathbf{x}, \tau)}{\Delta\tau} \quad (4.4-7)$$

by the backward difference method. After the process of the LRBFCM, we utilize the  $S^{ij}$  as the  $S$  whose given operator are the first partial spatial derivative with respect to  $x_i$  and  $x_j$  and transform the governing equations into the following linear system

$$\begin{bmatrix} \mathbf{A}_{11} - \frac{2\rho}{\Delta\tau^2} \mathbf{I} & \mathbf{A}_{12} & \mathbf{A}_{13} & \mathbf{A}_{14} & \mathbf{A}_{15} \\ \mathbf{A}_{21} & \mathbf{A}_{22} - \frac{2\rho}{\Delta\tau^2} \mathbf{I} & \mathbf{A}_{23} & \mathbf{A}_{24} & \mathbf{A}_{25} \\ \mathbf{A}_{31} & \mathbf{A}_{32} & \mathbf{A}_{33} - \frac{2\rho}{\Delta\tau^2} \mathbf{I} & \mathbf{A}_{34} & \mathbf{A}_{35} \\ \mathbf{A}_{41} & \mathbf{A}_{42} & \mathbf{A}_{43} & \mathbf{A}_{44} & \mathbf{A}_{45} \\ \mathbf{A}_{51} & \mathbf{A}_{52} & \mathbf{A}_{53} & \mathbf{A}_{54} & \mathbf{A}_{55} - \frac{1}{\Delta\tau} \mathbf{I} \end{bmatrix} \begin{Bmatrix} \boldsymbol{\alpha}^{u_1} \\ \boldsymbol{\alpha}^{u_2} \\ \boldsymbol{\alpha}^{u_3} \\ \boldsymbol{\alpha}^{\phi} \\ \boldsymbol{\alpha}^M \end{Bmatrix} = \begin{Bmatrix} \mathbf{B}_1 \\ \mathbf{B}_2 \\ \mathbf{B}_3 \\ \mathbf{B}_4 \\ \mathbf{B}_5 \end{Bmatrix}, \quad (4.4-8)$$

The governing equations for the transient analysis in Eq. (4.3-8) can be divided by several

parts, shown as follows.

$$\mathbf{A}_{11} = [c_{11}\mathbf{S}^{11} + c_{66}\mathbf{S}^{22} + c_{55}\mathbf{S}^{33}]_{N \times N}$$

$$\mathbf{A}_{21} = [(c_{12} + c_{66})\mathbf{S}^{12}]_{N \times N}$$

$$\mathbf{A}_{31} = [(c_{13} + c_{55})\mathbf{S}^{13}]_{N \times N}$$

$$\mathbf{A}_{41} = [(e_{15} + e_{31})\mathbf{S}^{13}]_{N \times N}$$

$$\mathbf{A}_{51} = [\mathbf{0}]_{N \times N}$$

$$\mathbf{A}_{13} = [(c_{13} + c_{55})\mathbf{S}^{13}]_{N \times N}$$

$$\mathbf{A}_{23} = [(c_{13} + c_{44})\mathbf{S}^{23}]_{N \times N}$$

$$\mathbf{A}_{33} = [c_{55}\mathbf{S}^{11} + c_{44}\mathbf{S}^{22} + c_{33}\mathbf{S}^{33}]_{N \times N}$$

$$\mathbf{A}_{43} = [e_{15}(\mathbf{S}^{11} + \mathbf{S}^{22}) + e_{33}\mathbf{S}^{33}]_{N \times N}$$

$$\mathbf{A}_{53} = [\mathbf{0}]_{N \times N}$$

$$\mathbf{A}_{15} = [\mathbf{0}]_{N \times N}$$

$$\mathbf{A}_{25} = [\mathbf{0}]_{N \times N}$$

$$\mathbf{A}_{35} = [\mathbf{0}]_{N \times N}$$

$$\mathbf{A}_{45} = [-q\mathbf{I}]_{N \times N}$$

$$\mathbf{A}_{55} = [d_{11}\mathbf{S}^{11} + d_{22}\mathbf{S}^{22} + d_{33}\mathbf{S}^{33}]_{N \times N}$$

$$\mathbf{A}_{12} = [(c_{12} + c_{66})\mathbf{S}^{12}]_{N \times N}$$

$$\mathbf{A}_{22} = [c_{66}\mathbf{S}^{11} + c_{11}\mathbf{S}^{22} + c_{44}\mathbf{S}^{33}]_{N \times N}$$

$$\mathbf{A}_{32} = [(c_{44} + c_{13})\mathbf{S}^{23}]_{N \times N}$$

$$\mathbf{A}_{42} = [(e_{15} + e_{31})\mathbf{S}^{23}]_{N \times N}$$

$$\mathbf{A}_{52} = [\mathbf{0}]_{N \times N}$$

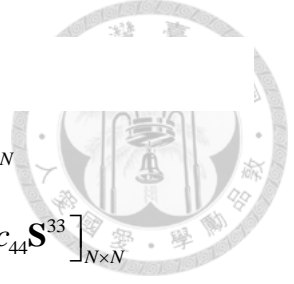
$$\mathbf{A}_{14} = [(e_{31} + e_{15})\mathbf{S}^{13}]_{N \times N}$$

$$\mathbf{A}_{24} = [(e_{31} + e_{15})\mathbf{S}^{23}]_{N \times N}$$

$$\mathbf{A}_{34} = [e_{15}(\mathbf{S}^{11} + \mathbf{S}^{22}) + e_{33}\mathbf{S}^{33}]_{N \times N}$$

$$\mathbf{A}_{44} = [-h_{11}\mathbf{S}^{11} - h_{11}\mathbf{S}^{22} - h_{33}\mathbf{S}^{33}]_{N \times N}$$

$$\mathbf{A}_{54} = [\mathbf{0}]_{N \times N}$$





$$\mathbf{B}_1 = -\frac{5\rho}{\Delta\tau^2}[\mathbf{u}_1(\tau)]_{N \times 1} + \frac{4\rho}{\Delta\tau^2}[\mathbf{u}_1(\tau - \Delta\tau)]_{N \times 1} - \frac{\rho}{\Delta\tau^2}[\mathbf{u}_1(\tau - 2\Delta\tau)]_{N \times 1}$$

$$\mathbf{B}_2 = -\frac{5\rho}{\Delta\tau^2}[\mathbf{u}_2(\tau)]_{N \times 1} + \frac{4\rho}{\Delta\tau^2}[\mathbf{u}_2(\tau - \Delta\tau)]_{N \times 1} - \frac{\rho}{\Delta\tau^2}[\mathbf{u}_2(\tau - 2\Delta\tau)]_{N \times 1}$$

$$\mathbf{B}_3 = -\frac{5\rho}{\Delta\tau^2}[\mathbf{u}_3(\tau)]_{N \times 1} + \frac{4\rho}{\Delta\tau^2}[\mathbf{u}_3(\tau - \Delta\tau)]_{N \times 1} - \frac{\rho}{\Delta\tau^2}[\mathbf{u}_3(\tau - 2\Delta\tau)]_{N \times 1}$$

$$\mathbf{B}_4 = [\mathbf{0}]_{N \times 1}$$

$$\mathbf{B}_5 = -\frac{1}{\Delta\tau}[\mathbf{M}(\tau)]_{N \times 1}$$

However, the approximation of the first-order temporal partial derivative term by the backward difference method is first-order accurate. It overshadows the second-order accurate approximation for the second-order temporal partial derivative terms by the Houbolt finite-difference scheme. Therefore, we also adopt the second-order accurate central difference for the first-order temporal partial derivative term and investigate the effects. The linear system of the governing equations is modified as:

$$\begin{bmatrix} \mathbf{A}_{11} - \frac{2\rho}{\Delta\tau^2} \mathbf{I} & \mathbf{A}_{12} & \mathbf{A}_{13} & \mathbf{A}_{14} & \mathbf{A}_{15} \\ \mathbf{A}_{21} & \mathbf{A}_{22} - \frac{2\rho}{\Delta\tau^2} \mathbf{I} & \mathbf{A}_{23} & \mathbf{A}_{24} & \mathbf{A}_{25} \\ \mathbf{A}_{31} & \mathbf{A}_{32} & \mathbf{A}_{33} - \frac{2\rho}{\Delta\tau^2} \mathbf{I} & \mathbf{A}_{34} & \mathbf{A}_{35} \\ \mathbf{A}_{41} & \mathbf{A}_{42} & \mathbf{A}_{43} & \mathbf{A}_{44} & \mathbf{A}_{45} \\ \mathbf{A}_{51} & \mathbf{A}_{52} & \mathbf{A}_{53} & \mathbf{A}_{54} & \mathbf{A}_{55} - \frac{1}{2\Delta\tau} \mathbf{I} \end{bmatrix} \begin{Bmatrix} \boldsymbol{\alpha}^{\mu_1} \\ \boldsymbol{\alpha}^{\mu_2} \\ \boldsymbol{\alpha}^{\mu_3} \\ \boldsymbol{\alpha}^{\phi} \\ \boldsymbol{\alpha}^M \end{Bmatrix} = \begin{Bmatrix} \mathbf{B}_1 \\ \mathbf{B}_2 \\ \mathbf{B}_3 \\ \mathbf{B}_4 \\ \mathbf{B}_5 \end{Bmatrix}, \quad (4.4-9)$$

The components in the linear system are exactly the same except  $\mathbf{B}_5$  as

$$\mathbf{B}_5 = -\frac{1}{2\Delta\tau}[\mathbf{M}(\tau - \Delta\tau)]_{N \times 1}$$



#### 4.4.2 The static analysis

For validation of the LRBFCM method, we analyze the static case and the governing equations become

$$\sigma_{ij,j}(\mathbf{x}, \tau) = 0, \quad (4.4-10)$$

$$D_{i,i}(\mathbf{x}, \tau) = qM(\mathbf{x}, \tau), \quad (4.4-11)$$

$$J_{i,i}(\mathbf{x}, \tau) = 0. \quad (4.4-12)$$

The linear system in Eq. (4.3-8) becomes

$$\begin{bmatrix} \mathbf{A}_{11} & \mathbf{A}_{12} & \mathbf{A}_{13} & \mathbf{A}_{14} & \mathbf{A}_{15} \\ \mathbf{A}_{21} & \mathbf{A}_{22} & \mathbf{A}_{23} & \mathbf{A}_{24} & \mathbf{A}_{25} \\ \mathbf{A}_{31} & \mathbf{A}_{32} & \mathbf{A}_{33} & \mathbf{A}_{34} & \mathbf{A}_{35} \\ \mathbf{A}_{41} & \mathbf{A}_{42} & \mathbf{A}_{43} & \mathbf{A}_{44} & \mathbf{A}_{45} \\ \mathbf{A}_{51} & \mathbf{A}_{52} & \mathbf{A}_{53} & \mathbf{A}_{54} & \mathbf{A}_{55} \end{bmatrix} \begin{Bmatrix} \boldsymbol{\alpha}^{\mu_1} \\ \boldsymbol{\alpha}^{\mu_2} \\ \boldsymbol{\alpha}^{\mu_3} \\ \boldsymbol{\alpha}^{\phi} \\ \boldsymbol{\alpha}^M \end{Bmatrix} = \{\mathbf{0}\}, \quad (4.4-13)$$

The governing equations for the static analysis in Eq. (4.3.10) can be divided by several parts, as shown below.

$$\mathbf{A}_{11} = [c_{11}\mathbf{S}^{11} + c_{66}\mathbf{S}^{22} + c_{55}\mathbf{S}^{33}]_{N \times N}$$

$$\mathbf{A}_{12} = [(c_{12} + c_{66})\mathbf{S}^{12}]_{N \times N}$$

$$\mathbf{A}_{21} = [(c_{12} + c_{66})\mathbf{S}^{12}]_{N \times N}$$

$$\mathbf{A}_{22} = [c_{66}\mathbf{S}^{11} + c_{11}\mathbf{S}^{22} + c_{44}\mathbf{S}^{33}]_{N \times N}$$

$$\mathbf{A}_{31} = [(c_{13} + c_{55})\mathbf{S}^{13}]_{N \times N}$$

$$\mathbf{A}_{32} = [(c_{44} + c_{13})\mathbf{S}^{23}]_{N \times N}$$

$$\mathbf{A}_{41} = [(e_{15} + e_{31})\mathbf{S}^{13}]_{N \times N}$$

$$\mathbf{A}_{42} = [(e_{15} + e_{31})\mathbf{S}^{23}]_{N \times N}$$

$$\mathbf{A}_{51} = [\mathbf{0}]_{N \times N}$$

$$\mathbf{A}_{52} = [\mathbf{0}]_{N \times N}$$

$$\mathbf{A}_{13} = \left[ (c_{13} + c_{55}) \mathbf{S}^{13} \right]_{N \times N}$$

$$\mathbf{A}_{23} = \left[ (c_{13} + c_{44}) \mathbf{S}^{23} \right]_{N \times N}$$

$$\mathbf{A}_{33} = \left[ c_{55} \mathbf{S}^{11} + c_{44} \mathbf{S}^{22} + c_{33} \mathbf{S}^{33} \right]_{N \times N}$$

$$\mathbf{A}_{43} = \left[ e_{15} (\mathbf{S}^{11} + \mathbf{S}^{22}) + e_{33} \mathbf{S}^{33} \right]_{N \times N}$$

$$\mathbf{A}_{53} = [\mathbf{0}]_{N \times N}$$

$$\mathbf{A}_{14} = \left[ (e_{31} + e_{15}) \mathbf{S}^{13} \right]_{N \times N}$$

$$\mathbf{A}_{24} = \left[ (e_{31} + e_{15}) \mathbf{S}^{23} \right]_{N \times N}$$

$$\mathbf{A}_{34} = \left[ e_{15} (\mathbf{S}^{11} + \mathbf{S}^{22}) + e_{33} \mathbf{S}^{33} \right]_{N \times N}$$

$$\mathbf{A}_{44} = \left[ -h_{11} \mathbf{S}^{11} - h_{11} \mathbf{S}^{22} - h_{33} \mathbf{S}^{33} \right]_{N \times N}$$

$$\mathbf{A}_{54} = [\mathbf{0}]_{N \times N}$$

$$\mathbf{A}_{15} = [\mathbf{0}]_{N \times N}$$

$$\mathbf{A}_{25} = [\mathbf{0}]_{N \times N}$$

$$\mathbf{A}_{35} = [\mathbf{0}]_{N \times N}$$

$$\mathbf{A}_{45} = [-q\mathbf{I}]_{N \times N}$$

$$\mathbf{A}_{43} = \left[ e_{15} (\mathbf{S}^{11} + \mathbf{S}^{22}) + e_{33} \mathbf{S}^{33} \right]_{N \times N}$$

$$\mathbf{A}_{55} = \left[ d_{11} \mathbf{S}^{11} + d_{22} \mathbf{S}^{22} + d_{33} \mathbf{S}^{33} \right]_{N \times N}$$

## 4.5 Numerical examples

In this section we first verify the presented LRBFCM by comparing the results of the LRBFCM with those of the FEM. The FEM solutions are taken from the commercial software, COMSOL. The computational domain is shown in Fig.4.5.1.



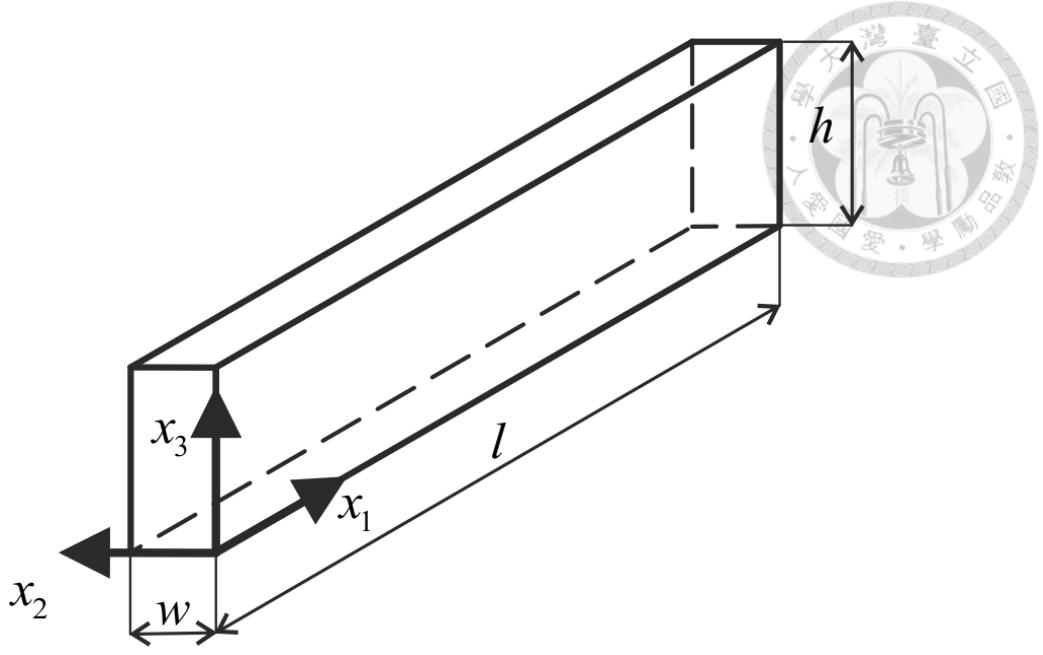


Fig.4.5.1 The geometry of the beam.

The length  $l$  , width  $w$  , and height  $h$  are 0.1 m, 0.005 m, and 0.01 m, respectively.

The material properties for aluminum nitride (AlN) [70] are considered for the homogeneous ( $\delta = 0$ ) and shown as below.

$$c_{11}^{(0)} = c_{22}^{(0)} = 4.03 \times 10^{11} \text{ Nm}^{-2}, c_{12}^{(0)} = 1.43 \times 10^{11} \text{ Nm}^{-2}, c_{13}^{(0)} = c_{23}^{(0)} = 1.04 \times 10^{11} \text{ Nm}^{-2},$$

$$c_{33}^{(0)} = 3.82 \times 10^{11} \text{ Nm}^{-2}, c_{44}^{(0)} = c_{55}^{(0)} = 1.20 \times 10^{11} \text{ Nm}^{-2},$$

$$e_{15}^{(0)} = -0.39 \text{ Cm}^{-2}, e_{31}^{(0)} = -0.66 \text{ Cm}^{-2}, e_{33}^{(0)} = 1.57 \text{ Cm}^{-2},$$

$$h_{11}^{(0)} = h_{22}^{(0)} = h_{33}^{(0)} = 8.092 \times 10^{-11} \text{ C(mV)}^{-1},$$

$$\mu_{11} = \mu_{22} = \mu_{33} = 3.0 \times 10^{-2} \text{ m}^2 (\text{Vs})^{-1},$$

$$d_{11} = d_{22} = d_{33} = 7.0 \times 10^{-4} \text{ m}^2 \text{ s}^{-1},$$

$$\rho = 3255 \text{ kgm}^{-3}, q = 1.602 \times 10^{-19} \text{ C}, M_0 = 1.0 \times 10^6 \text{ m}^{-3}.$$

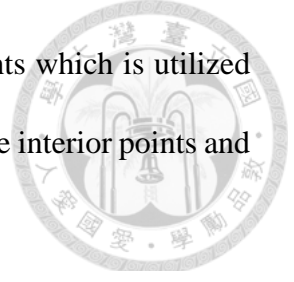


Fig.4.5.2 shows the structured distribution of 2805 ( $51 \times 5 \times 11$ ) points which is utilized to approximate the variables. The red points and the blue points denote interior points and boundary points, respectively.

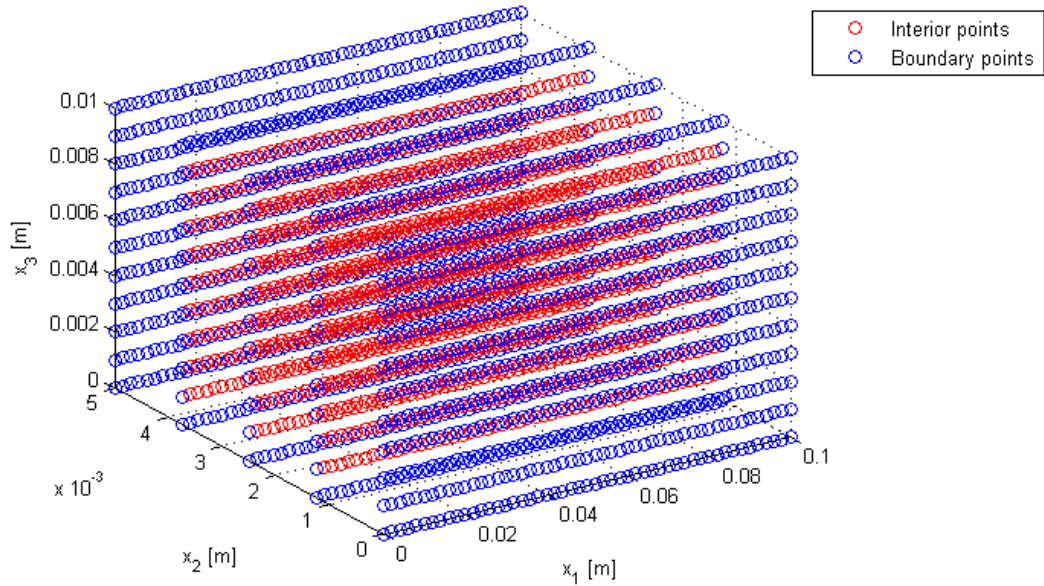


Fig.4.5.2 The distribution of the points.

In the numerical example, a uniform static compressive load at the top of the analyzed beam is considered. All the prescribed boundary conditions are given as follows:

$$\begin{aligned}
 \tilde{\mathbf{t}}(\mathbf{x}) = 0 \quad \quad \tilde{\mathbf{Q}}(\mathbf{x}) = \tilde{\mathbf{S}}(\mathbf{x}) = 0 & \quad \text{at } \mathbf{x} \in \Gamma|_{x_1=0} \cup \Gamma|_{x_1=l} \\
 \tilde{\mathbf{t}}(\mathbf{x}) = 0, \quad \quad \tilde{\mathbf{Q}}(\mathbf{x}) = \tilde{\mathbf{S}}(\mathbf{x}) = 0 & \quad \text{at } \mathbf{x} \in \Gamma|_{x_2=0} \cup \Gamma|_{x_2=w} \\
 \tilde{\mathbf{t}}(\mathbf{x}) = 0, \quad \quad \tilde{\phi}(\mathbf{x}) = \tilde{\mathbf{M}}(\mathbf{x}) = 0 & \quad \text{at } \mathbf{x} \in \Gamma|_{x_3=0} \\
 \tilde{t}_3(\mathbf{x}) = 100\text{Pa}, \quad \tilde{t}_1(\mathbf{x}) = \tilde{t}_2(\mathbf{x}) = \tilde{\mathbf{Q}}(\mathbf{x}) = \tilde{\mathbf{S}}(\mathbf{x}) = 0 & \quad \text{at } \mathbf{x} \in \Gamma|_{x_3=h}
 \end{aligned}$$

Furthermore, taking into account the symmetry and in order to eliminate the rigid body motion,  $\tilde{u}_3(\mathbf{x}) = 0$  at  $\mathbf{x} \in \Gamma|_{x_1=0} \cup \Gamma|_{x_1=l}$  ;  $\tilde{u}_1(\mathbf{x}) = \tilde{u}_2(\mathbf{x}) = 0$  at  $\mathbf{x} \in \Gamma|_{x_1=0, x_3=h/2} \cup \Gamma|_{x_1=l, x_3=h/2}$  are assumed and the vanishing initial values are imposed on

the initial conditions.

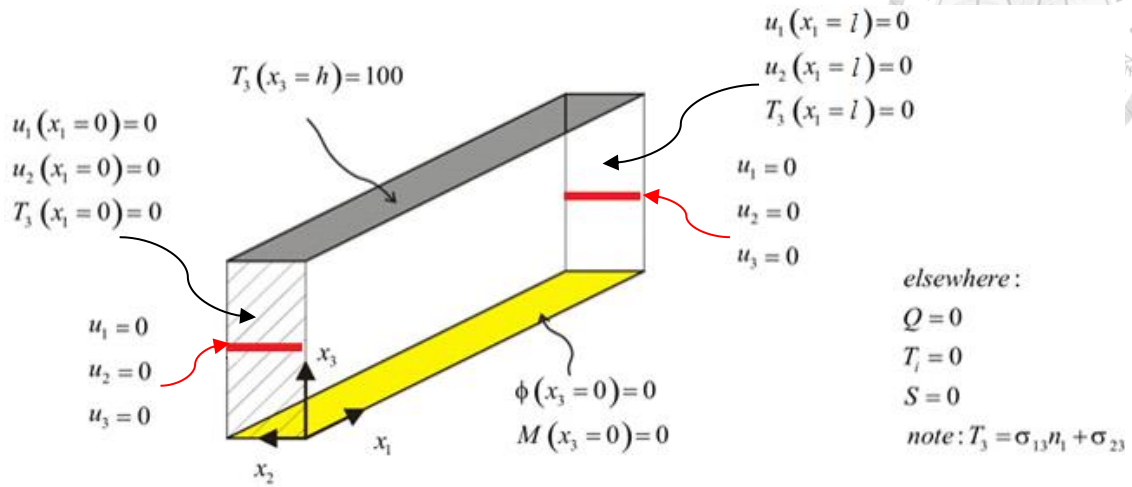


Fig.4.5.3 The illustration of the boundary conditions.

#### 4.5.1 The validation of the LRBFCM

We compare the benchmark FEM-COMSOL results obtained by 9353 tetrahedral elements for the line along  $x_1$  and located at  $x_2=0$  and  $x_3=h/2$  with those of the LRBFCM. The variation of displacement in direction 3, electric potential, and electron density are shown in Fig.4.5.1.1-3, and the three different values of uniform static compressive load at the top of the beam are prescribed in this numerical analysis.

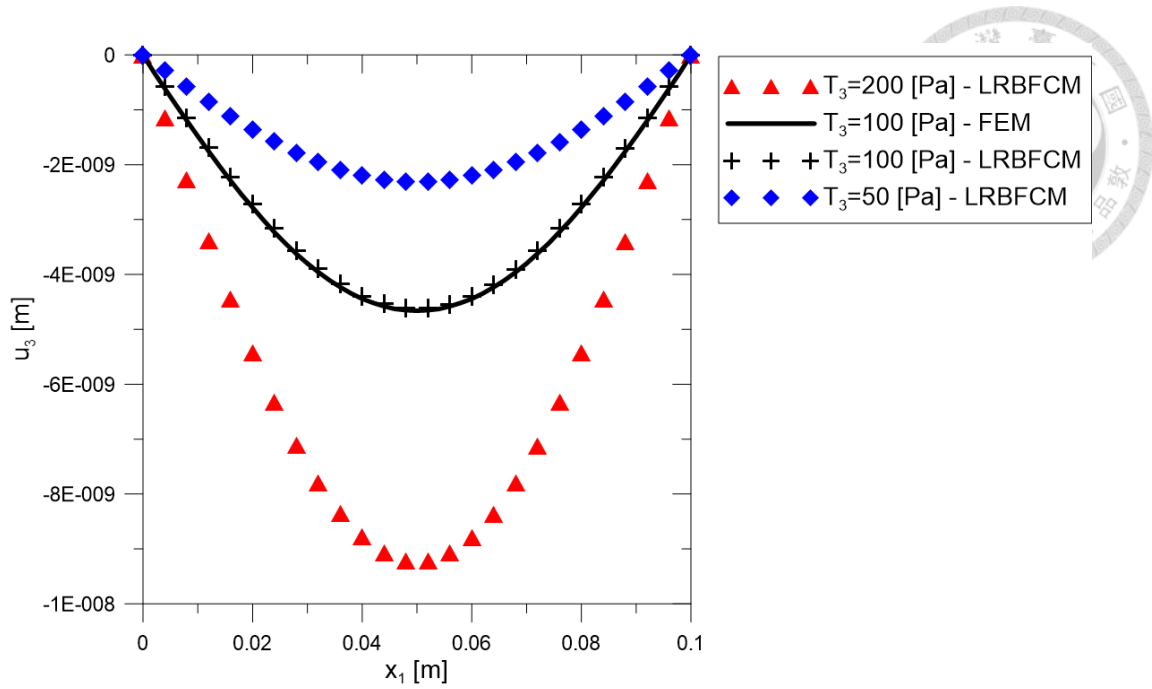


Fig.4.5.1.1 Variation of vertical displacement for a line along  $x_1$  and located at  $x_2 = 0$  and  $x_3 = h/2$  in the static analysis.

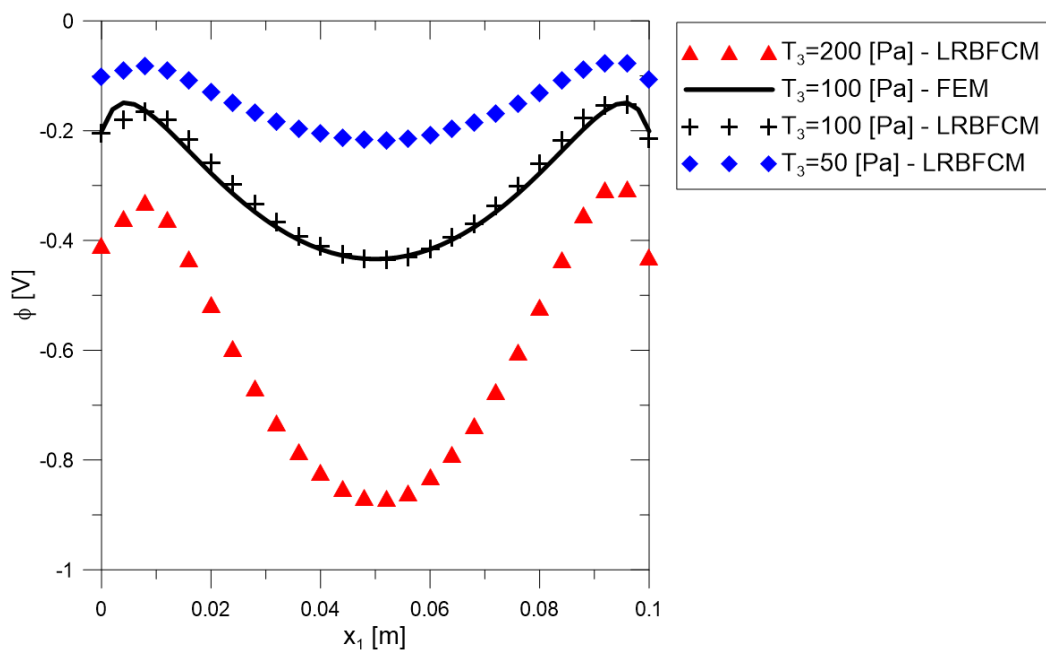


Fig.4.5.1.2 Variation of electric potential for a line along  $x_1$  and located at  $x_2 = 0$  and  $x_3 = h/2$  in the static analysis.

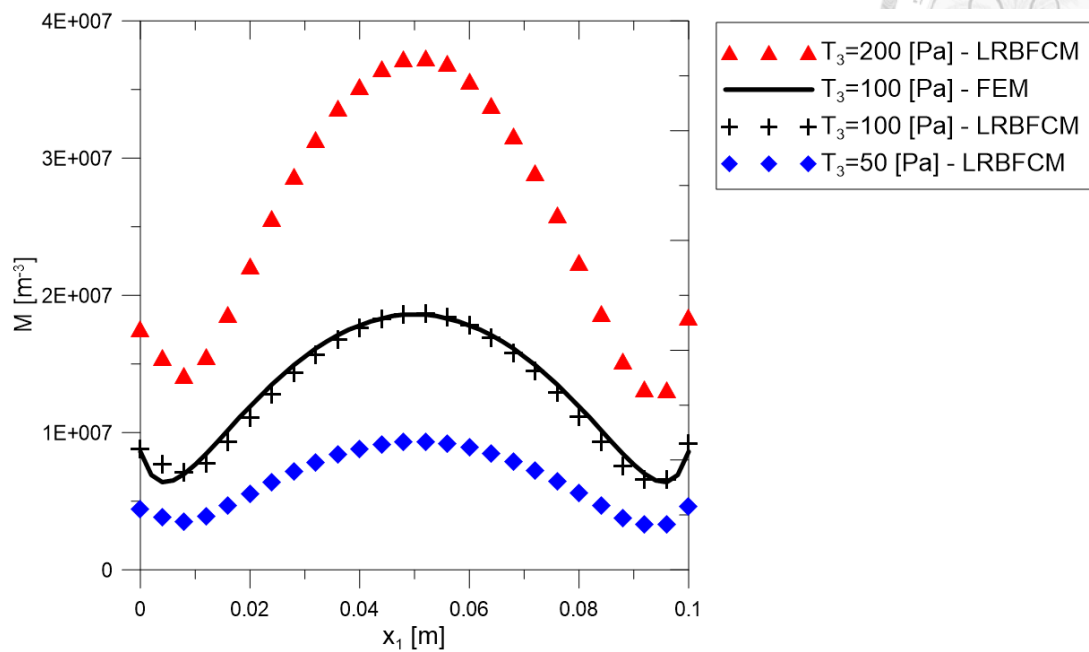
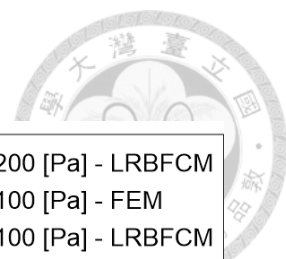


Fig.4.5.1.3 Variation of electron density for a line along  $x_1$  and located at  $x_2 = 0$  and  $x_3 = h/2$  in the static analysis.

From the above comparisons, the LRBFCM results agree well with the benchmark FEM results obtained in the static analysis for a homogeneous beam. The increasing bending of the beam, induced electric potential, and electron density are observed with the increasing value of the uniform static compressive load.

### 4.5.2 The influence of initial electron density

Then, the influence of the initial electron density is investigated in this subsection. It is shown that the initial electron density plays an important role in the electron density in Fig.4.5.2.3, while, the slight effects on the vertical displacement and the electric potential are observed in Fig.4.5.2.1-3.

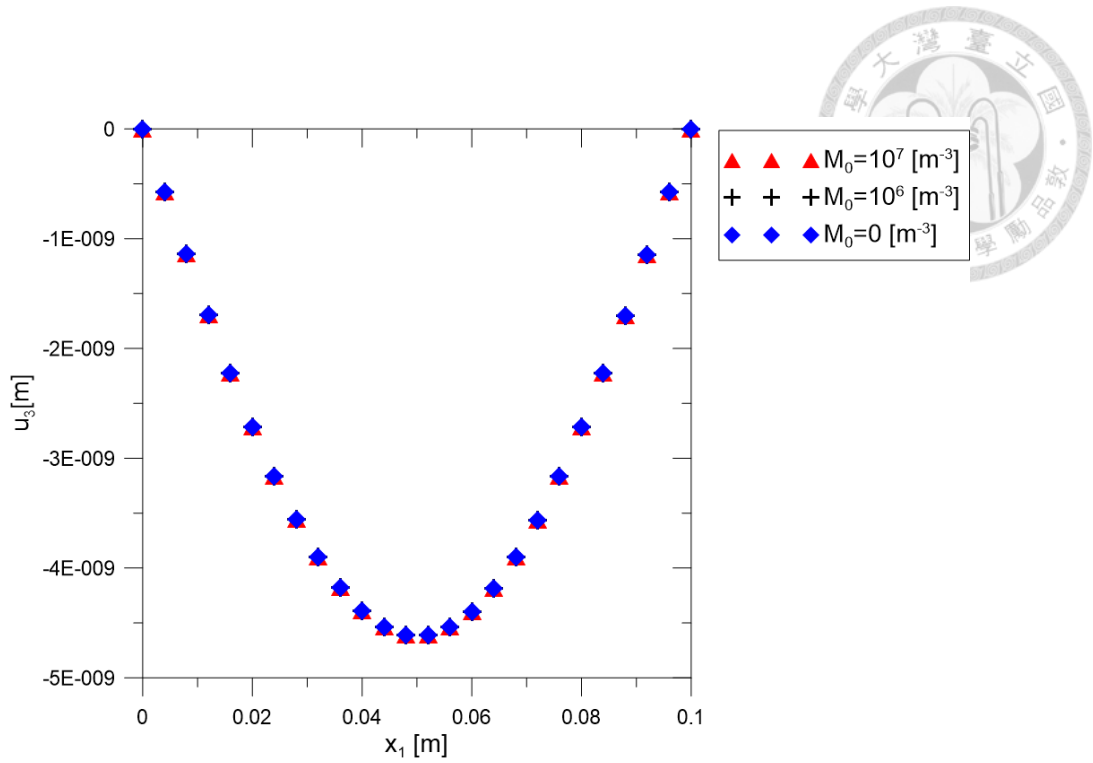


Fig.4.5.2.1 Variation of vertical displacements along the line  $(x_1, x_2 = 0, x_3 = h/2)$  for different values of  $M_0$  in the beam under static load  $T_3 = 100\text{Pa}$ .

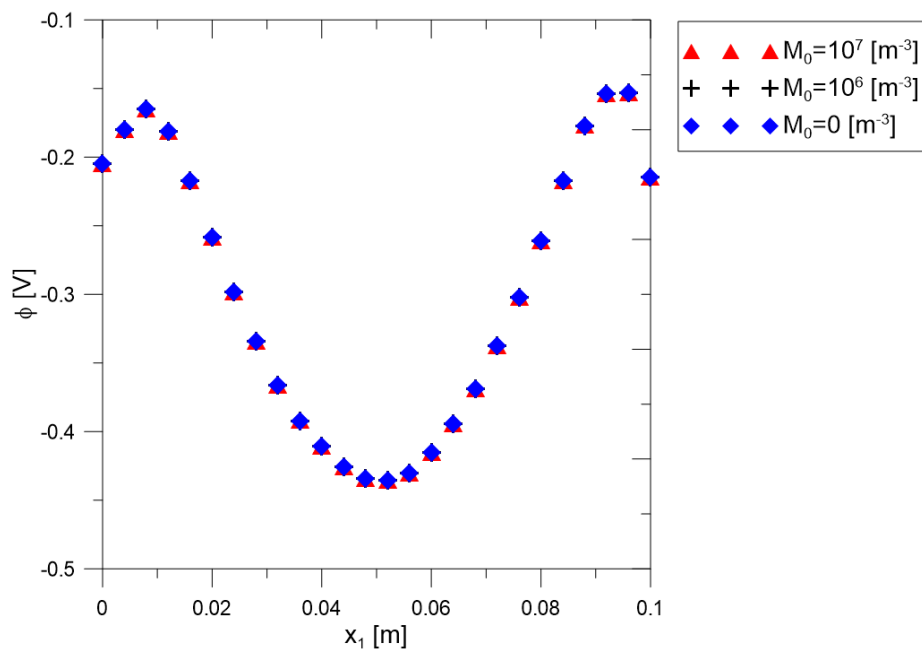


Fig.4.5.2.2 Variation of electric potential along the line  $(x_1, x_2 = 0, x_3 = h/2)$  for different values of  $M_0$  in the beam under static load  $T_3 = 100\text{Pa}$ .

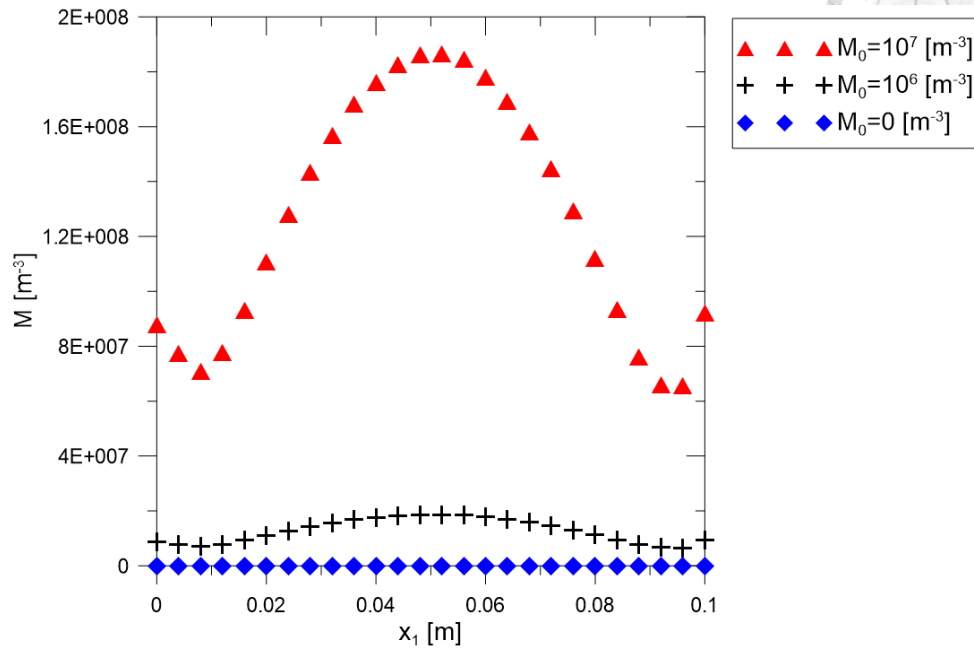
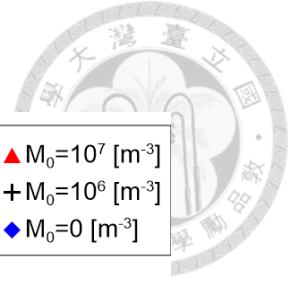


Fig.4.5.2.3 Variation of electron density along the line  $(x_1, x_2 = 0, x_3 = h/2)$  for different values of  $M_0$  in the beam under static load  $T_3 = 100\text{Pa}$  .

Since the value of the electric charge of electron is quite small in comparison with the other material coefficients, the mechanical fields and electric potential in Eqs. (4.2-14)-(4.2-17) are affected slightly by the change of the electron density. However, the electron density highly relies on the value of the initial electron density in Eq. (4.2-18).

### 4.5.3 The influence of grading parameter

In this subsection, the influence of grading properties  $\delta$  in Eq. (4.2-24), the elastic, piezoelectric, and dielectric coefficients, on the response to the uniform static compressive load  $T_3 = 100\text{Pa}$  with the initial electron density  $M_0 = 1.0 \times 10^6 \text{ m}^{-3}$  are analyzed in Fig.4.5.3.1-3.

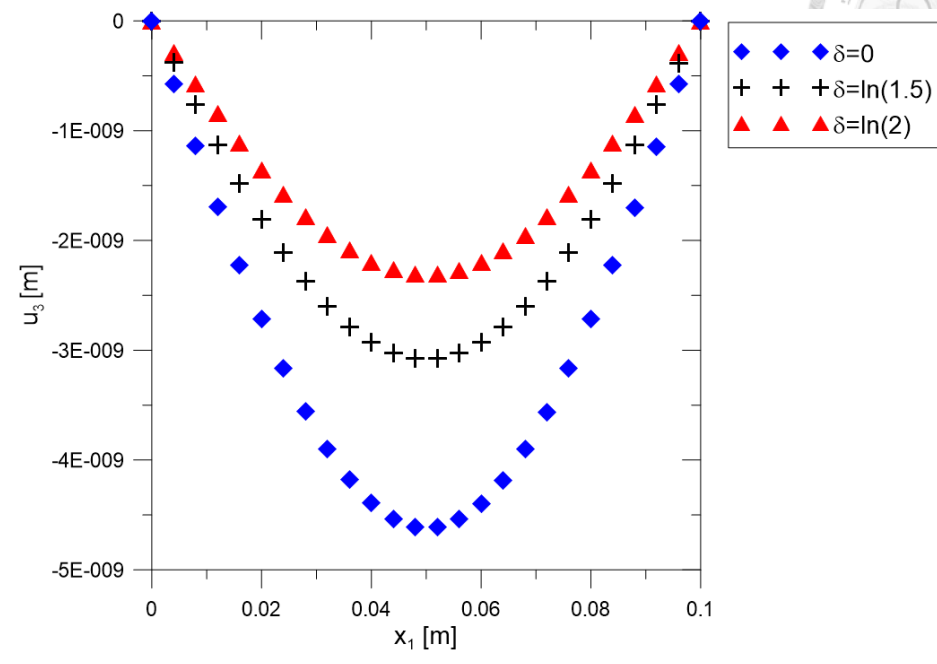
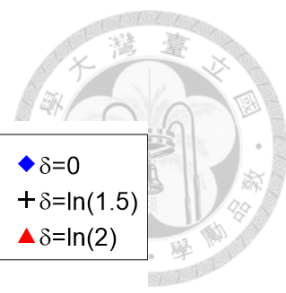


Fig.4.5.3.1 Variation of vertical displacement along the line  $(x_1, x_2 = 0, x_3 = h/2)$  for different values of the gradation parameter  $\delta$  in the FGM beam under the static load  $T_3 = 100\text{Pa}$ .

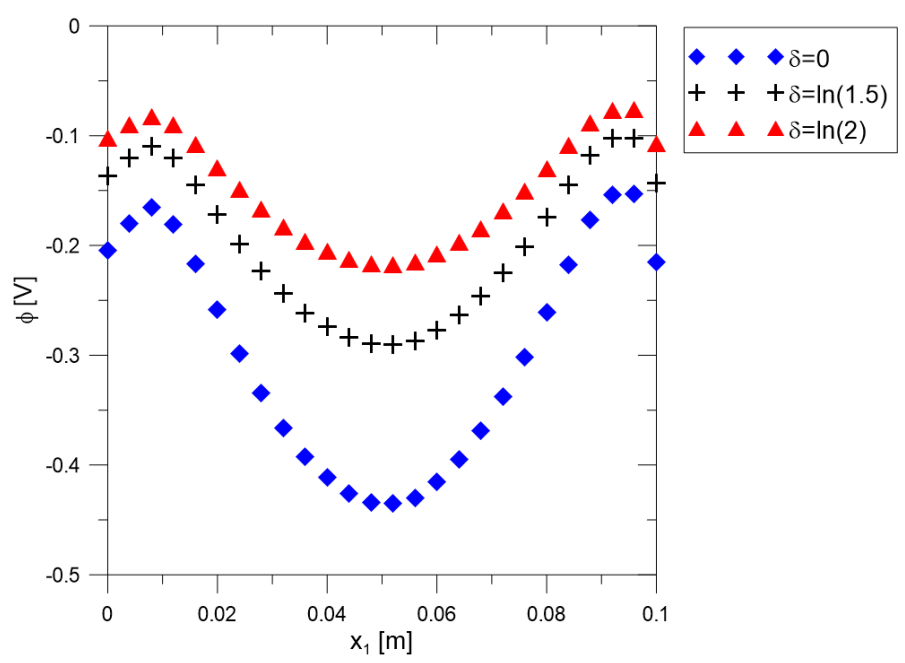
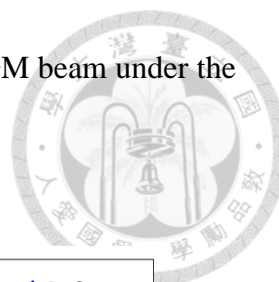


Fig.4.5.3.2 Variation of electric potential along the line  $(x_1, x_2 = 0, x_3 = h/2)$  for





different values of the gradation parameter  $\delta$  in the FGM beam under the static load  $T_3 = 100\text{Pa}$ .

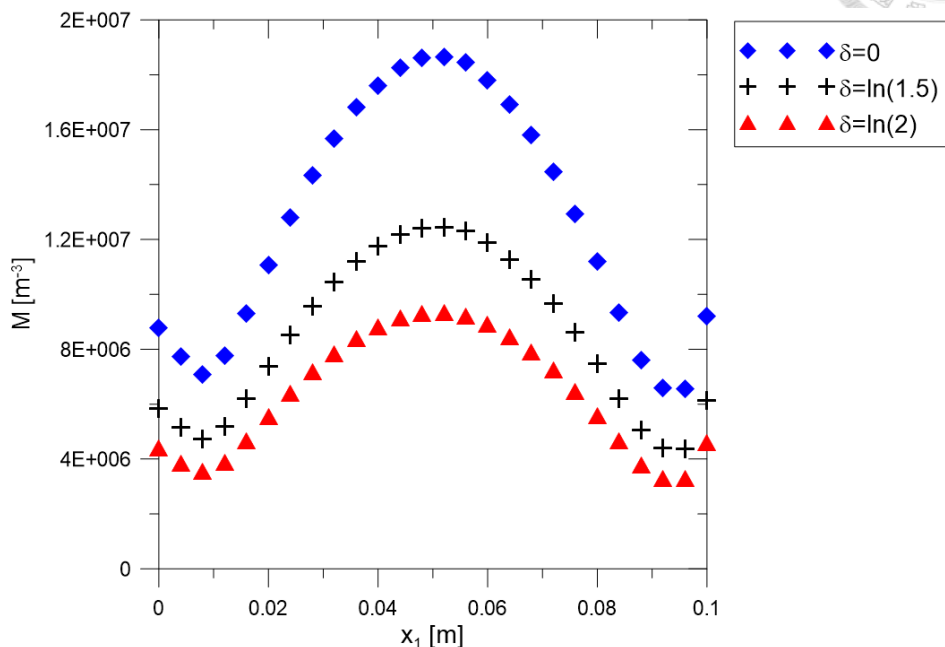


Fig.4.5.3.3 Variation of electron density along the line  $(x_1, x_2 = 0, x_3 = h/2)$  for different values of the gradation parameter  $\delta$  in the FGM beam under the static load  $T_3 = 100\text{Pa}$ .

It is observed that the increasing value of the gradation parameter  $\delta$  of the elastic, piezoelectric, and dielectric coefficients yields decreasing response of the vertical displacement, electric potential and electron density.

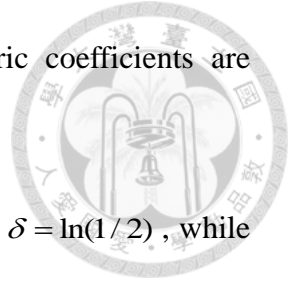
#### 4.5.4 The influence of complex grading parameter

In the subsection, the three combinations of the gradation of material coefficients in the FGM beam:

- (i) #1 - the grading parameters of the elastic coefficients, piezoelectric coefficients, and dielectric coefficients are  $\delta = \ln(2)$  ;
- (ii) #2 - the grading parameter of the dielectric coefficients  $\delta = \ln(1/2)$  , while

the grading parameters of the elastic and piezoelectric coefficients are  $\delta = \ln(2)$  ;

- (iii) #3 - the grading parameter of the dielectric coefficients  $\delta = \ln(1/2)$  , while the grading parameters of the elastic and piezoelectric coefficients are homogeneous ( $\delta = 0$ ) .



The comparisons of the numerical results are shown in Fig.4.5.4.1-3.

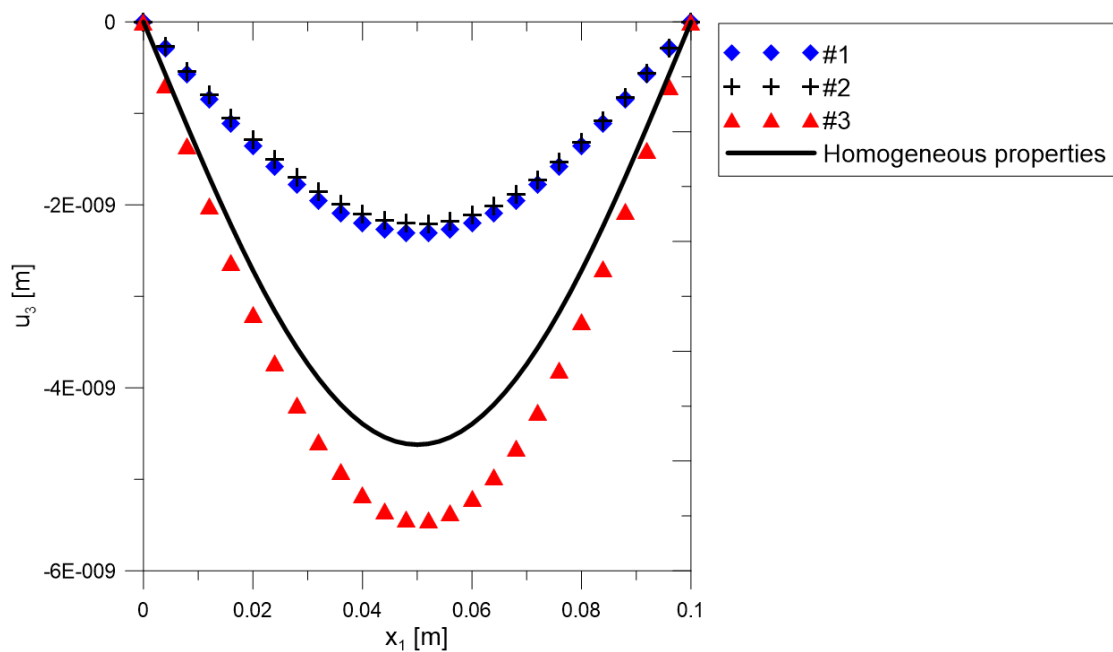


Fig.4.5.4.1 Variation of vertical displacement along the line ( $x_1, x_2 = 0, x_3 = h/2$ ) for the three combinations of the gradation of material coefficients in the FGM beam under static load  $T_3 = 100\text{Pa}$  .

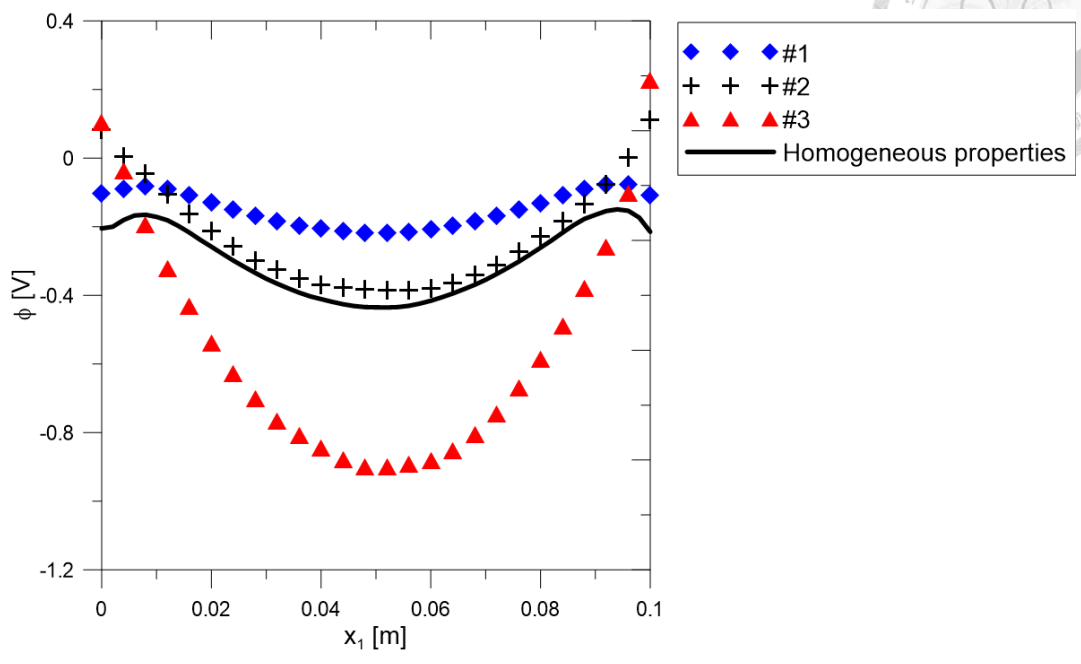


Fig.4.5.4.2 Variation of electric potential along the line  $(x_1, x_2 = 0, x_3 = h/2)$  for the three combinations of the gradation of material coefficients in the FGM beam under static load  $T_3 = 100\text{Pa}$ .

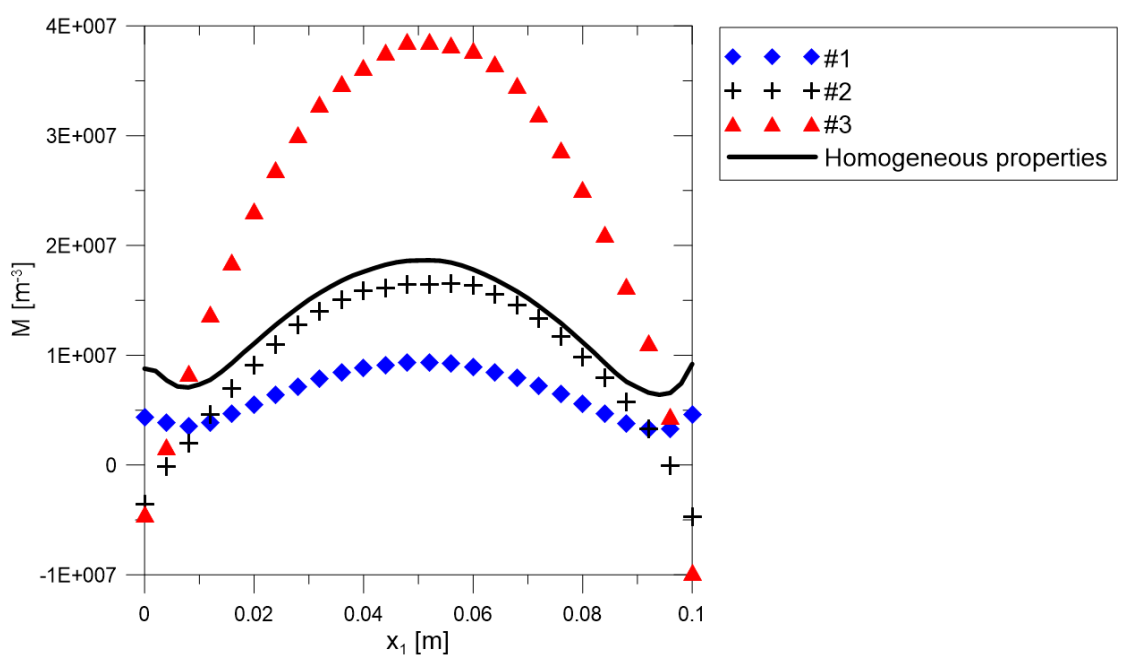


Fig.4.5.4.3 Variation of electron density along the line  $(x_1, x_2 = 0, x_3 = h/2)$  for

the three combinations of the gradation of material coefficients in the FGM beam under static load  $T_3 = 100\text{Pa}$  .

From the above results, the vertical displacement in homogeneous beam is much smaller than that in cases #1 and #2, while the effect on the electric potential and electron density is less distinctive in these two cases. In the case #2, the larger electrical outputs are observed near the beam ends ( $x_1 = 0$  and  $x_1 = l$ ) . The larger electrical outputs and vertical displacement compared with those in the homogeneous beam are observed in the case #3.

#### **4.5.5 The transient analyses**

The transient analysis is analyzed with the compressive impact load uniformly distributed on the top of the beam. The same boundary conditions as those in the static case are considered with the vanishing initial conditions including the initial electron density. The total computational time interval is composed of 77 time steps with the size of the time step  $\Delta\tau = 6.5 \times 10^{-6}$  [sec]. Due to the difference of accuracy for the first- and second-order temporal partial derivatives, the approximations of central-time (CT) and backward-time (BT) methods in time are investigated as shown in Fig.4.5.5.1-2.

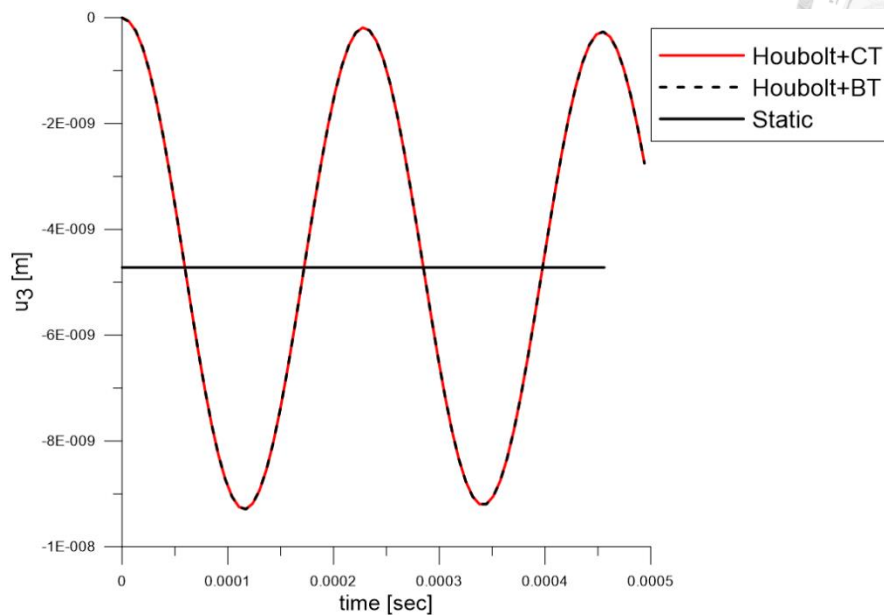
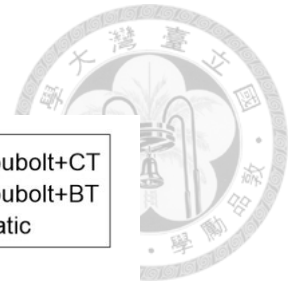


Fig.4.5.5.1 Time evolution of vertical displacement along the line  $(x_1, x_2 = 0, x_3 = h/2)$  by the CT and BT methods for the first-order temporal partial derivative under static and impact load  $T_3 = 100\text{Pa}$  .

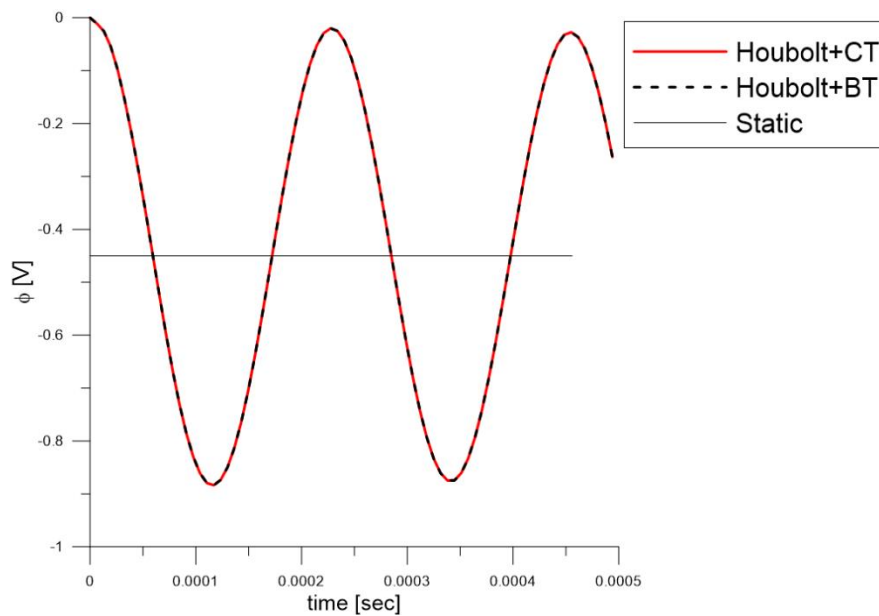
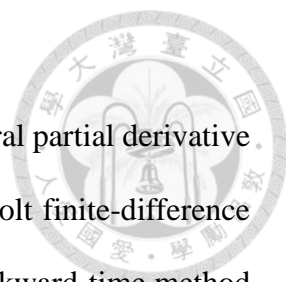


Fig.4.5.5.2 Time evolution of electric potential along the line  $(x_1, x_2 = 0, x_3 = h/2)$  by the CT and BT methods for the first-order temporal partial derivative



under static and impact load  $T_3 = 100\text{Pa}$  .

From the results by the CT and BT methods for the first-order temporal partial derivative we observed that there is almost no difference. Therefore, the Houbolt finite-difference scheme for the second-order temporal partial derivatives and the backward-time method for the first-order temporal partial derivative are applied in the following transient analyses. Fig.4.5.5.3-4 show the comparisons of the numerical results for the vertical displacement and electric potential at the point  $(x_1 = l/2; x_2 = 0; x_3 = h/2)$  obtained in the static analysis and transient analyses with the homogeneous properties and three combinations of the gradation of material coefficients in the FGM beams.

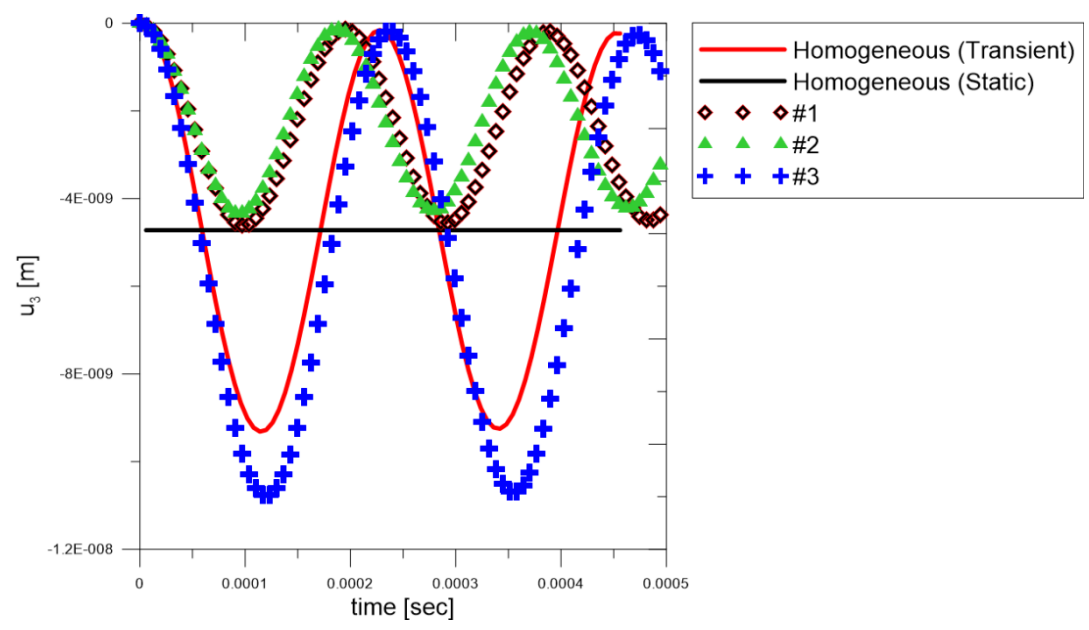


Fig.4.5.5.3 Time evolution of vertical displacement along the line  $(x_1, x_2 = 0, x_3 = h/2)$  for the three combinations of the gradation of material coefficients in the FGM beam under static and impact load  $T_3 = 100\text{Pa}$  .

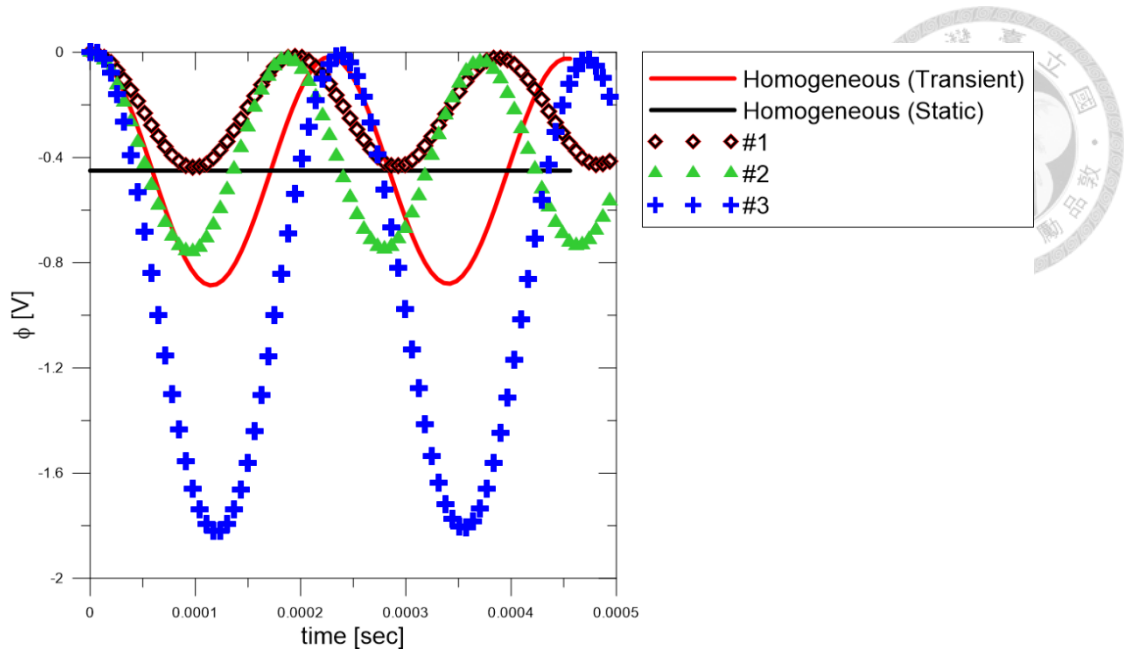


Fig.4.5.5.4 Time evolution of electric potential along the line  $(x_1, x_2 = 0, x_3 = h/2)$  for the three combinations of the gradation of material coefficients in the FGM beam under static and impact load  $T_3 = 100\text{Pa}$  .

It is observed that the transient responses at the point  $(x_1 = l/2; x_2 = 0; x_3 = h/2)$  oscillate around the static values (hence the amplitudes are equal to the static values). Additionally, the peak values of the vertical displacement in #1 and #2 are approximately half of that in the homogeneous properties. The peak values of the electric potential in #1 and #2 are slightly smaller than those in the homogeneous properties. Although #3 performs slightly larger displacement with respect to the homogeneous case, it increases almost twice peak values of electric potential.

## Chapter 5 Conclusions and Future Works



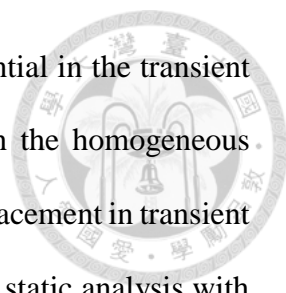
### 5.1 Conclusions

The proposed meshless method, the LRBFCM, is investigated and developed to analyze three-dimensional functionally graded piezoelectric semiconductors problems in this thesis. The FEM results obtained by the commercial software, COMSOL, are compared with the LRBFCM results and in good agreement in the static analysis for an analyzed beam with homogeneous material properties. Furthermore, the LRBFCM shows that the larger uniform static compressive load at the top of the beam results in the larger mechanical response and electrical outputs. The influence of initial electron density is also investigated. In comparison with the induced electron density, the resulting mechanical displacement and induced electric potential have small influence on the initial electron density.

Subsequently, since the LRBFCM performs the simplicity of prescribing spatial variation of material properties, an exponential gradation of material properties along the height of the FGM piezoelectric beam is prescribed and analyzed in numerical examples. It is observed that the lower mechanical displacement resulting from the increasing grading parameter of the elastic, piezoelectric, and dielectric coefficients. In addition, we analyze the three combinations of the gradation of material coefficients in the FGM beam. Among the three cases, the decreasing gradation of dielectric coefficients which contributes to the larger electrical outputs is observed and utilizing this characteristic could reduce the stress concentration of piezoelectric devices.

Ultimately, the transient analyses are investigated with vanishing initial conditions and initial electron density in the homogeneous and FGM piezoelectric beams. The results





show that the peak values of vertical displacement and electric potential in the transient analysis are two times larger than those in the static analysis with the homogeneous material properties. By the use of grading properties, the vertical displacement in transient analyses can be lowered to the half and be increased to the double in static analysis with the homogeneous properties.

The strong form meshless method is first applied in the analysis of general 3-D piezoelectric semiconductor solids in this thesis. The LRBFCM is an alternative numerical method and promising to be extended to complex problems in the future.

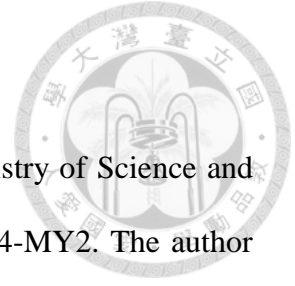
## **5.2 Future Works**

The LRBFCM is proved that it is advantageous to address the complicated engineering problems which geometrical scales in three dimensional and scales of values of material properties are very different. Therefore, the following topics are expected to analyze.


1. The non-uniform compressive load at the top of the beam can be considered to test the response of the piezoelectric equipment.
2. The piezoelectric materials which have the pyroelectric effect are expected to investigate. (In many piezoelectric materials an electric outputs is generated if temperature variations are applied. This effect is called as the pyroelectric phenomenon.)

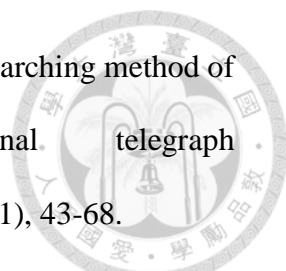
## **Acknowledgement**

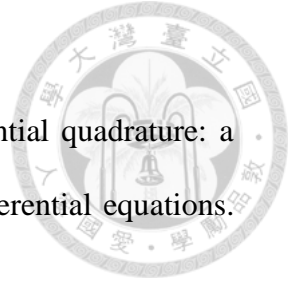
The author is grateful for the financial supports from the Ministry of Science and Technology of Taiwan under the grant number 103-2923-E-002-004-MY2. The author also appreciates the supports by the group of Professors Sladek and the Slovak Science and Technology Assistance Agency for the supports registered under number APVV-14-0216.



## References

- 
- [1] Gingold, R. A., & Monaghan, J. J. (1977). Smoothed particle hydrodynamics: theory and application to non-spherical stars. *Monthly Notices of the Royal Astronomical Society*, 181(3), 375-389.
- [2] Hardy, R. L. (1971). Multiquadric equations of topography and other irregular surfaces. *Journal of Geophysical Research*, 76(8), 1905-1915.
- [3] Kansa, E. J. (1990a). Multiquadrics—a scattered data approximation scheme with applications to computational fluid-dynamics—I surface approximations and partial derivative estimates. *Computers & Mathematics with Applications*, 19(8), 127-145.
- [4] Kansa, E. J. (1990b). Multiquadrics—A scattered data approximation scheme with applications to computational fluid-dynamics—II solutions to parabolic, hyperbolic and elliptic partial differential equations. *Computers & Mathematics with Applications*, 19(8), 147-161.
- [5] Golberg, M. A., Chen, C. S., & Karur, S. R. (1996). Improved multiquadric approximation for partial differential equations. *Engineering Analysis with Boundary Elements*, 18(1), 9-17.
- [6] Li, J., Hon, Y. C., & Chen, C. S. (2002). Numerical comparisons of two meshless methods using radial basis functions. *Engineering Analysis with Boundary Elements*, 26(3), 205-225.
- [7] Kupradze, V. D., & Aleksidze, M. A. (1964). The method of functional equations for the approximate solution of certain boundary value problems. *USSR Computational Mathematics and Mathematical Physics*, 4(4), 82-126.

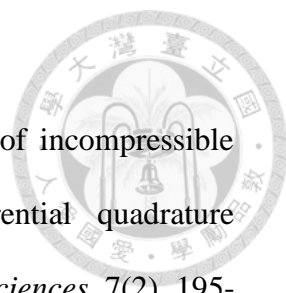
- 
- [8] Lin, C. Y., Gu, M. H., & Young, D. L. (2010). The time-marching method of fundamental solutions for multi-dimensional telegraph equations. *Computers, Materials & Continua (CMC)*, 18(1), 43-68.
- [9] Young, D. L., Lin, Y. C., Fan, C. M., & Chiu, C. L. (2009). The method of fundamental solutions for solving incompressible Navier–Stokes problems. *Engineering analysis with boundary elements*, 33(8), 1031-1044.
- [10] Chen, C. S., Karageorghis, A., & Smyrlis, Y. S. (Eds.). (2008). *The method of fundamental solutions: a meshless method* (pp. 299-321). Atlanta: Dynamic Publishers.
- [11] Fox, L., Henrici, P., & Moler, C. (1967). Approximations and bounds for eigenvalues of elliptic operators. *SIAM Journal on Numerical Analysis*, 4(1), 89-102.
- [12] Tsai, C. C., Chen, C. S., & Hsu, T. W. (2009). The method of particular solutions for solving axisymmetric polyharmonic and poly-Helmholtz equations. *Engineering Analysis with Boundary Elements*, 33(12), 1396-1402.
- [13] Wen, P. H., & Chen, C. S. (2010). The method of particular solutions for solving scalar wave equations. *International Journal for Numerical Methods in Biomedical Engineering*, 26(12), 1878-1889.
- [14] Chen, C. S., Fan, C. M., & Wen, P. H. (2011). The method of approximate particular solutions for solving elliptic problems with variable coefficients. *International Journal of Computational Methods*, 8(03), 545-559.
- [15] Bellman, R., & Casti, J. (1971). Differential quadrature and long-term integration. *Journal of Mathematical Analysis and Applications*, 34(2), 235-

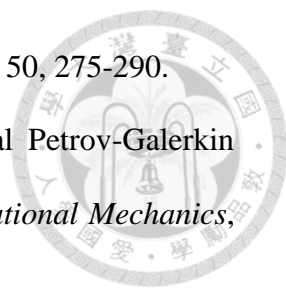



238.

- [16] Bellman, R., Kashef, B. G., & Casti, J. (1972). Differential quadrature: a technique for the rapid solution of nonlinear partial differential equations. *Journal of Computational Physics*, 10(1), 40-52.
- [17] Fu, Z. J., Chen, W., & Yang, H. T. (2013). Boundary particle method for Laplace transformed time fractional diffusion equations. *Journal of Computational Physics*, 235, 52-66.
- [18] Onate, E., Idelsohn, S., Zienkiewicz, O. C., & Taylor, R. L. (1996). A finite point method in computational mechanics. Applications to convective transport and fluid flow. *International Journal for Numerical Methods in Engineering*, 39(22), 3839-3866.
- [19] Lee, C. K., Liu, X., & Fan, S. C. (2003). Local multiquadric approximation for solving boundary value problems. *Computational Mechanics*, 30(5-6), 396-409.
- [20] Yao, G., Kolibal, J., & Chen, C. S. (2011). A localized approach for the method of approximate particular solutions. *Computers and Mathematics with Applications*, 61(9), 2376-2387.
- [21] Lin, C. Y., Gu, M. H., Young, D. L., & Chen, C. S. (2014). Localized method of approximate particular solutions with Cole–Hopf transformation for multi-dimensional Burgers equations. *Engineering Analysis with Boundary Elements*, 40, 78-92.
- [22] Lin, C. Y., Gu, M. H., Young, D. L., Sladek, J., & Sladek, V. (2015). The localized method of approximated particular solutions for solving two-dimensional incompressible viscous flow field. *Engineering Analysis with*

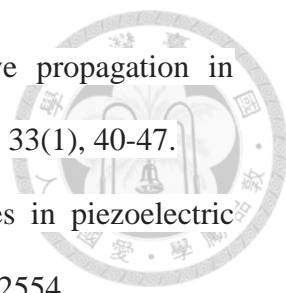
*Boundary Elements*, 57, 23-36.

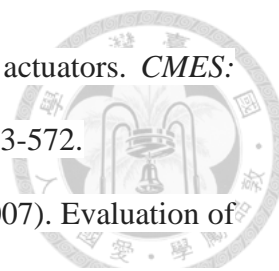
- 
- [23] Shu, C., Ding, H., & Yeo, K. S. (2005). Computation of incompressible Navier-Stokes equations by local RBF-based differential quadrature method. *CMES: Computer Modeling in Engineering & Sciences*, 7(2), 195-206.
- [24] Shen, L. H., Tseng, K. H., & Young, D. L. (2013). Evaluation of multi-order derivatives by local radial basis function differential quadrature method. *Journal of Mechanics*, 29(01), 67-78.
- [25] Chen, C. S., Brebbia, C. A., & Power, H. (1999). Dual reciprocity method using compactly supported radial basis functions. *Communications in Numerical Methods in Engineering*, 15(2), 137-150.
- [26] Šarler, B., & Vertnik, R. (2006). Meshfree explicit local radial basis function collocation method for diffusion problems. *Computers & Mathematics with Applications*, 51(8), 1269-1282.
- [27] Vertnik, R., & Šarler, B. (2006). Meshless local radial basis function collocation method for convective-diffusive solid-liquid phase change problems. *International Journal of Numerical Methods for Heat & Fluid Flow*, 16(5), 617-640.
- [28] Fan, C. M., Chen, C. S., Chan, H. F., & Chiu, C. L. (2013). The local RBF collocation method for solving the double-diffusive natural convection in fluid-saturated porous media. *International Journal of Heat and Mass Transfer*, 57(2), 500-503.
- [29] Chou, C. K., Sun, C. P., Young, D. L., Sladek, J., & Sladek, V. (2015). Extrapolated local radial basis function collocation method for shallow water

- 
- problems. *Engineering Analysis with Boundary Elements*, 50, 275-290.
- [30] Atluri, S. N., & Zhu, T. (1998). A new meshless local Petrov-Galerkin (MLPG) approach in computational mechanics. *Computational Mechanics*, 22(2), 117-127.
- [31] Atluri, S. N. (2004). *The meshless method (MLPG) for domain & BIE discretizations* (Vol. 677). Forsyth: Tech Science Press.
- [32] Franke, R. (1982). Scattered data interpolation: Tests of some methods. *Mathematics of Computation*, 38(157), 181-200.
- [33] Yao, G., Šarler, B., & Chen, C. S. (2011). A comparison of three explicit local meshless methods using radial basis functions. *Engineering Analysis with Boundary Elements*, 35(3), 600-609.
- [34] Curie, J., & Curie, P. (1880). Développement, par pression, de l'électricité polaire dans les cristaux hémihédres à faces inclinées. *Comptes Rendus*, 91, 294-295.
- [35] Lippmann, G. (1908). Epreuves reversibles. Photographies intégrales. *Comptes-Rendus Academie des Sciences*, 146, 446-451.
- [36] Flatau, A. B., & Chong, K. P. (2002). Dynamic smart material and structural systems. *Engineering Structures*, 24(3), 261-270.
- [37] Wang, Q., & Wang, C. M. (2001). A controllability index for optimal design of piezoelectric actuators in vibration control of beam structures. *Journal of Sound and Vibration*, 242(3), 507-518.
- [38] Hagood, N. W., & von Flotow, A. (1991). Damping of structural vibrations with piezoelectric materials and passive electrical networks. *Journal of Sound and Vibration*, 146(2), 243-268.

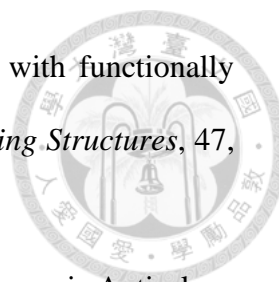
- 
- [39] Song, G., Sethi, V., & Li, H. N. (2006). Vibration control of civil structures using piezoceramic smart materials: A review. *Engineering Structures*, 28(11), 1513-1524.
- [40] Giurgiutiu, V. (2005). Tuned Lamb wave excitation and detection with piezoelectric wafer active sensors for structural health monitoring. *Journal of Intelligent Material Systems and Structures*, 16(4), 291-305.
- [41] Erturk, A. (2011). Piezoelectric energy harvesting for civil infrastructure system applications: Moving loads and surface strain fluctuations. *Journal of Intelligent Material Systems and Structures*, 22(17), 1959-1973.
- [42] Wu, C., Kahn, M., & Moy, W. (1996). Piezoelectric ceramics with functional gradients: a new application in material design. *Journal of the American Ceramic Society*, 79(3), 809-812.
- [43] Suresh, S., & Mortensen, A. (1998). *Fundamentals of Functionally Graded Materials*. The Institute of Materials, London.
- [44] Paulino, G. H., Jin, Z. H., & Dodds Jr, R. H. (2003). Failure of functionally graded materials. *Comprehensive Structural Integrity*, 2(13), 607-644.
- [45] Li, C., & Weng, G. J. (2002). Antiplane crack problem in functionally graded piezoelectric materials. *Journal of Applied Mechanics*, 69(4), 481-488.
- [46] Zhu, X., Wang, Q., & Meng, Z. (1995). A functionally gradient piezoelectric actuator prepared by powder metallurgical process in PNN-PZ-PT system. *Journal of Materials Science Letters*, 14(7), 516-518.
- [47] Ikeda, T. (1990). *Fundamentals of piezoelectricity*. Oxford University Press, Oxford.



- 
- [48] Hutson, A. R., & White, D. L. (1962). Elastic wave propagation in piezoelectric semiconductors. *Journal of Applied Physics*, 33(1), 40-47.
- [49] White, D. L. (1962). Amplification of ultrasonic waves in piezoelectric semiconductors. *Journal of Applied Physics*, 33(8), 2547-2554.
- [50] Heyman, J. S. (1978). Phase insensitive acoustoelectric transducer. *The Journal of the Acoustical Society of America*, 64(1), 243-249.
- [51] Busse, L. J., & Miller, J. G. (1981). Response characteristics of a finite aperture, phase insensitive ultrasonic receiver based upon the acoustoelectric effect. *The Journal of the Acoustical Society of America*, 70(5), 1370-1376.
- [52] De Lorenzi, H. G., & Tiersten, H. F. (1975). On the interaction of the electromagnetic field with heat conducting deformable semiconductors. *Journal of Mathematical Physics*, 16(4), 938-957
- [53] Maugin, G. A., & Daher, N. (1986). Phenomenological theory of elastic semiconductors. *International Journal of Engineering Science*, 24(5), 703-731.
- [54] Chen, Y. H., Ma, J., & Li, T. (2004). Electrophoretic deposition and characterization of a piezoelectric FGM monomorph actuator. *Ceramics International*, 30(7), 1807-1809.
- [55] Ohs, R. R., & Aluru, N. R. (2001). Meshless analysis of piezoelectric devices. *Computational Mechanics*, 27(1), 23-36.
- [56] Sladek, J., Sladek, V., Stanak, P., & Pan, E. (2010). The MLPG for bending of electroelastic plates. *CMES: Computer Modeling in Engineering & Sciences*, 64(3), 267-297.
- [57] Sladek, J., Sladek, V., Stanak, P., Wen, P. H., & Atluri, S. N. (2012).



- Laminated elastic plates with piezoelectric sensors and actuators. *CMES: Computer Modeling in Engineering & Sciences*, 85(6), 543-572.
- [58] Sladek, J., Sladek, V., Zhang, C., Solec, P., & Pan, E. (2007). Evaluation of fracture parameters in continuously nonhomogeneous piezoelectric solids. *International Journal of Fracture*, 145(4), 313-326.
- [59] Nguyen, V. P., Rabczuk, T., Bordas, S., & Duflot, M. (2008). Meshless methods: a review and computer implementation aspects. *Mathematics and Computers in Simulation*, 79(3), 763-813.
- [60] Sladek, J., Stanak, P., Han, Z. D., Sladek, V., & Atluri, S. N. (2013a). Applications of the MLPG method in engineering & sciences: a review. *Comput. Model. Eng. Sci*, 92, 423-475.
- [61] Liew, K. M., Lim, H. K., Tan, M. J., & He, X. Q. (2002). Analysis of laminated composite beams and plates with piezoelectric patches using the element-free Galerkin method. *Computational Mechanics*, 29(6), 486-497.
- [62] Sladek, J., Sladek, V., & Solec, P. (2009). Elastic analysis in 3D anisotropic functionally graded solids by the MLPG. *CMES: Computer Modeling in Engineering and Sciences*, 43(3), 223.
- [63] Stanak, P., Tadeu, A., Sladek, J., & Sladek, V. (2015). Meshless analysis of piezoelectric sensor embedded in composite floor panel. *Journal of Intelligent Material Systems and Structures*, 26(15), 2092-2107.
- [64] Sladek, J., Sladek, V., Solec, P., & Saez, A. (2008). Dynamic 3D axisymmetric problems in continuously non-homogeneous piezoelectric solids. *International Journal of Solids and Structures*, 45(16), 4523-4542.
- [65] Sladek, J., Sladek, V., Stanak, P., Zhang, C., & Wünsche, M. (2013b).



Analysis of the bending of circular piezoelectric plates with functionally graded material properties by a MLPG method. *Engineering Structures*, 47, 81-89.

- [66] Sladek, J., Sladek, V., Pan, E., & Young, D. L. (2014a). Dynamic Anti-plane Crack Analysis in Functional Graded Piezoelectric Semiconductor Crystals. *CMES: Computer Modeling in Engineering & Sciences*, 99(4), 273-296.
- [67] Sladek, J., Sladek, V., Pan, E., & Wünsche, M. (2014b). Fracture analysis in piezoelectric semiconductors under a thermal load. *Engineering Fracture Mechanics*, 126, 27-39.
- [68] Chiang, Y. C. (2015), Piezoelectric Sensors and Quasicrystal Plate Problems by Localized Radial Basis Function Collocation Method, *Master Thesis*, National Taiwan University, Taipei, Taiwan.
- [69] Houbolt J.C. (1950) A recurrence matrix solution for the dynamic response of elastic aircraft. *Journal of Aeronautical Sciences*, 17, 371-376.
- [70] Auld, B. A. (1973). *Acoustic fields and waves in solids*. John Wiley and Sons, New York.

# Appendix



## A. Houbolt method

For the second-order temporal derivatives, the Houbolt method is second-order accurate, and the derivation is shown as follows:

$$\ddot{F}_{\tau+\Delta\tau} \cong \frac{2F_{\tau+\Delta\tau} - 5F_{\tau} + 4F_{\tau-\Delta\tau} - F_{\tau-2\Delta\tau}}{(\Delta\tau)^2}$$

$$F_{\tau} = F_{\tau+\Delta\tau} - \frac{\Delta\tau}{1!} \frac{\partial F}{\partial \tau} \Big|_{\tau+\Delta\tau} + \frac{(\Delta\tau)^2}{2!} \frac{\partial^2 F}{\partial \tau^2} \Big|_{\tau+\Delta\tau} - \frac{(\Delta\tau)^3}{3!} \frac{\partial^3 F}{\partial \tau^3} \Big|_{\tau+\Delta\tau} + \frac{(\Delta\tau)^4}{4!} \frac{\partial^4 F}{\partial \tau^4} \Big|_{\tau+\Delta\tau} + \dots$$

$$F_{\tau-\Delta\tau} = F_{\tau+\Delta\tau} - \frac{2\Delta\tau}{1!} \frac{\partial F}{\partial \tau} \Big|_{\tau+\Delta\tau} + \frac{(2\Delta\tau)^2}{2!} \frac{\partial^2 F}{\partial \tau^2} \Big|_{\tau+\Delta\tau} - \frac{(2\Delta\tau)^3}{3!} \frac{\partial^3 F}{\partial \tau^3} \Big|_{\tau+\Delta\tau} + \frac{(2\Delta\tau)^4}{4!} \frac{\partial^4 F}{\partial \tau^4} \Big|_{\tau+\Delta\tau} + \dots$$

$$F_{\tau-2\Delta\tau} = F_{\tau+\Delta\tau} - \frac{3\Delta\tau}{1!} \frac{\partial F}{\partial \tau} \Big|_{\tau+\Delta\tau} + \frac{(3\Delta\tau)^2}{2!} \frac{\partial^2 F}{\partial \tau^2} \Big|_{\tau+\Delta\tau} - \frac{(3\Delta\tau)^3}{3!} \frac{\partial^3 F}{\partial \tau^3} \Big|_{\tau+\Delta\tau} + \frac{(3\Delta\tau)^4}{4!} \frac{\partial^4 F}{\partial \tau^4} \Big|_{\tau+\Delta\tau} + \dots$$

$$\ddot{F}_{\tau+\Delta\tau} = \frac{2F_{\tau+\Delta\tau} - 5F_{\tau} + 4F_{\tau-\Delta\tau} - F_{\tau-2\Delta\tau}}{(\Delta\tau)^2} + \left( \frac{11}{16} \frac{\partial^4 F}{\partial \tau^4} \Big|_{\tau+\Delta\tau} \right) (\Delta\tau)^2 + \dots$$

## Personal Information



**Name:** 陸學賢 / Hubert Hsueh-Hsien Lu

**Birthday:** 1992/06/28

**E-mail:** r03521324@ntu.edu.tw  
kn7419533@gmail.com

## Education background

高雄市私立道明高級中學 (2007~2010)

國立成功大學水利工程學系學士 (2010~2014)

國立台灣大學土木工程研究所水利工程組碩士(2014~2016)

## Publications



### (a) Journal Paper

1. Lu, H. H.-H., Young, D. L., Sladek, J., & Sladek, V. (2016). Three-dimensional analysis for functionally graded piezoelectric semiconductors. (In revision)

### (b) Conference Paper

1. Lu, H.-H., & Young, D. L. (2014). Alternative splitting approaches for Stokes flow problem by multiquadrics method, 2014 Proceedings of the 31st National Conference on Mechanical Engineering of CSME, Taichung, Taiwan.
2. Lu, H. H.-H., Young, D. L., Sladek, J., & Sladek, V. (2016). Three-dimensional analysis of functionally graded thermo-piezoelectricity problems by the local radial basis function collocation method, the 7th International Conference on Computational Methods (ICCM2016), Berkeley, CA, USA.
3. Sladek, J., Sladek, V., Lu, H. H.-H., & Young, D. L. (2016). Three-dimensional analyses of piezoelectric semiconductor problems, the Chinese Conference on Computational Mechanics in conjunction with International Symposium on Computational Mechanics' 2016 (CCCM – ISCM 2016), Hangzhou, China.